Density-functional tight-binding modeling of electromechanics of phosphorene

Pro gradu, 5.2.2018

Author:

Antti Pihlajamäki

Supervisor:

Pekka Koskinen

JYVÄSKYLÄN YLIOPISTO
FYSIIKAN LAITOS

Acknowledgements

Thank you for my supervisor Pekka Koskinen. His guidance and advice have greatly improved my writing and this thesis. Thank you for the Department of Physics of University of Jyväskylä. They made it possible for me to start my thesis in summer 2017. I also thank all of those who have listened my explanation commenting, advising or just nodding understandingly.

Abstract

Pihlajamäki, Antti
Density-functional tight-binding modeling of electromechanics of phosphorene
Master's thesis
Department of Physics, University of Jyväskylä, 2018, 63 pages.

Single-layer black phosphorus or phosphorene is a two-dimensional material made from a puckered honeycomb structure. It is a semiconductor with a tunable band gap and both its mechanical and electronic properties are highly asymmetric because of the puckering. Recently there has been numerous computational studies and some experimental works trying to bring deeper understanding about this relatively new 2D material. In this study we simulate phosphorene using computationally low-cost density functional tight-binding (DFTB) method to see how stretching, shearing and bending affect its electronic properties. The band structure analysis shows that there is a relation between shearing and bending. This discovery is a confirmation for the relation between earlier theoretical predictions concerning bending and the computational results about shearing.

Keywords: Phosphorene, DFTB, band structure, bending, shear

Abstrakti

Pihlajamäki, Antti
Fosforeenin eletromekaaniset ominaisuudet mallinnettuna tiheysfunktionaaliteoriaan perustuvalla tiukan sidoksen mallilla
Maisterin tutkielma
Fysiikan laitos, Jyväskylän yliopisto, 2018, 63 sivua.

Musta fosfori koostuu kaksiulotteisista kerroksista samaan tapaan kuin grafiitti. Siksipä yksittäistä mustan fosforin kerrosta kutsutaan fosforeeniksi. Fosforeeni on taipuneiden kuusikulmioiden muodostama verkkorakenne. Se muistuttaa hieman grafeenin rakennetta. Fosforeeni on tutkimuskohteena verrattain uusi kaksiuloitteinen materiaali, vaikka musta fosfori onkin tunnettu jo pitkään yhtenä fosforin allotrooppina. Kyseessä on puolijohde, jonka vyöaukkoa voidaan muokata. Esimerkiksi elastiset deformaatiot ja kerrosten lukumäärä vaikuttavat vyöaukon kokoon ja suoruuteen k-avaruudessa. Kaikki fosforeenin ominaisuudet ovat erittäin asymmetrisiä johtuen rakenteen aaltoilevuudesta.

Tässä tutkielmassa simuloimme fosforeenia käyttäen tiheysfunktionaaliteoriaan perustuvaa tiukan sidoksen mallia (DFTB). Kyseessä on laskennallisesti kevyt menetelmä, joka pohjautuu tunnetusti tarkkaan tiheysfunktionaaliteoriaan. Muodostimme fosforeenille parametrisoinnin menetelmäämme varten. Tämän jälkeen tarkastelimme venymän, leikkausmyötymän ja taivutuksen vaikutusta fosforeenin elektronirakenteeseen. Vyörakenteiden analysointi osoitti, että taivutusten ja leikkausmyötymien välillä on yhteys. Aiemmissa tutkimuksissa on esitetty, että taivutusten matemaattiseen esitykseen sisältyy leikkausmyötymiin liittyviä termejä. Leikkausmyötymien on taas laskennallisesti havaittu vaikuttavan degeneroituneisiin energiavöihin. Me havaitsimme taivutusten aiheuttavan samanlaisia muutoksia kyseisissä energiavöissä.

Avainsanat: Fosforeeni, DFTB, vyörakenne, taivutus, leikkausmyötymä

Contents

1 Introduction

Phosphorus is an abundant element in nature. Minerals, animal tissues and plants all contain phosphorus in some form [1, pp.486]. Elemental phosphorus has several allotropic forms. White phosphorus has a tetrahedral atomic structure and red phophorus has chains formed by tetrahedrons, to mention some forms. Black phophorus, on the other hand, is 2D-material. The atoms are arranged to puckered layers with a honeycomb structure, as seen in the figure 1. The armchair (ac) direction is along y axis and the zigzag (zz) direction is along x axis.

Black phosphorus was fabricated first time in 1914 by P. W. Bridgman as a byproduct of an experiment [2] but the real interest towards it has awaken quite recently. Black phosphorus is a layered material like graphite. A single layer of black phosphorus is often called phosphorene in a similar fashion as a single layer of graphite is called graphene. The lattice is orthorhombic and the unit cell contains four atoms. Although phosphorene might seem to have similarities with graphene, they are significantly different. Unlike flat graphene, puckering makes phosphorene and its properties highly anisotropic.

Graphene doesn't have a band gap [3, 4] and this limits its possible applications. Phosphorene on the other hand is a semiconductor with a direct band gap. Tran *et al.* point out that the band gap is slightly indirect, but the difference is so small that it can be considered to be direct and located in Γ point [5]. In addition to this the band gap is also tunable. There are several parameters that can tune it. Tran *et al.* have studied computationally using *ab initio* methods how the amount of layers affect to the band gap [5]. They reported that, depending on the method the band gap can vary from 0.3 eV of the bulk to about 2.0 eV of the single layer phosphorene. Experimentally it has been determined that the band gap of the single layer phosphorene is 1.45 eV [6].

Not just the number of layers affect to electronic properties of the phosphorene but also stretching, bending, shear and strain. Furthermore, all these deformations are dependent on the direction because of the anisotropic structure. Usually these properties are studied in ac- and zz-direction but the intermediate directions also

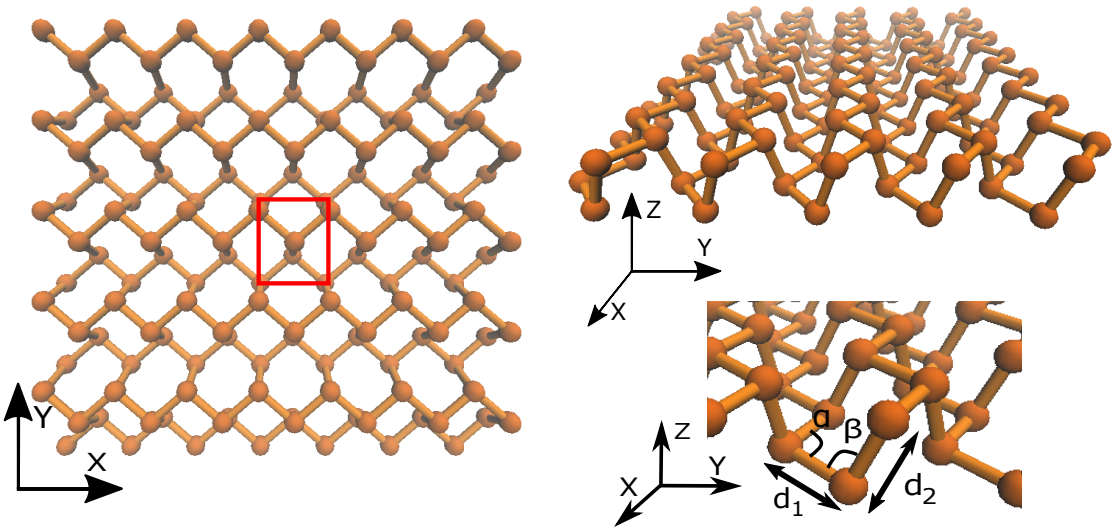

Figure 1. The phosphorene sheet is constructed by puckered hexagons. The red box shows the unit cell which contains four atoms. On the lower right there is shown different bond lengths and angles. The armchair (ac) direction is along y axis and the zigzag (zz) direction is along x axis.

provide interesting phenomena as seen in this study. There are numerous studies about these deformations and their effects on the band structure of phosphorene. They are referred to in section 3 while comparing corresponding values.

Black phosphorus is an interesting semiconductor, because its band gap can be tuned. The size of the band gap determines the applications of the semiconducting material. It is especially important for transistors, which are one of the possible applications of black phosphorus. There have been several studies about black phosphorus FETs. Li *et al.* report that the thickness of the black phosphorus crystal (number of phosphorene layers) affect its conducting properties [7]. Buscema *et al.* have used thin layers of black phosphorus to create photoresponsive FETs [8]. Xia, Wang and Jia studied extensively the properties of black phosphorus for optoelectronics and electronics [9]. They realized that anisotropy is a significant factor in this kind of applications.

In addition to the band gap, also other properties of black phosphorus seem to be promising for its possible application. Andres Castellanos-Gomez points out well that it ‘‘bridges the bap between graphene and transition metal dichalcogenides’’

[10]. He has collected figures presenting different properties important for electronics. These are, for example, carrier mobility, current on/off ratio, and resistivity. In all aspects black phosphorus is a compromise between these two types of materials.

Black phosphorus is a promising material but its few layer form has a property that limits its possible applications. Even though black phosphorus is the most inert phosphorus allotrope, its few-layer form reacts easily with air and moisture and forms oxides [11]. P_4O_{10} is the most important phosphorus oxide and it is hydrophilic [1, pp. 526-527]. Water causes the reaction

$$P_4O_{10} + 6H_2O \longrightarrow 4H_3PO_4.$$

Oxygen defects and their effect on phosphorene has been studied by Ziletti *et al.* [12]. In order to prevent these defects, phosphorene needs to be encapsulated to prevent it from getting into a contact with air [13].

Here we studied phosphorene computationally. Phosphorene sheet was subjected to different elastic deformations and the behavior of its electronic structure was monitored. The computational method used in this study is density-functional tight-binding (DFTB). It is not an *ab initio* method like its ''big brother'' full density-functional theory (DFT) because it needs some pre-calculated or measured information about the system. Information needs to be given in a suitable form so that computational machinery can use it. This is why before the actual computations we make so-called parametrization.

Parametrization contains several system-specific parameters about the electronic properties and repulsive interactions within the system. During the parametrization process many often-used numerical values are stored. This way there is no need to compute everything from the scratch making computations significantly less demanding. In order to be sure that our parameters describe the system well we need reference material for comparison. We used Verma *et al.* results [14] as a key reference. This is a natural choice because our methods are somewhat similar. We used revised periodic boundary conditions (RPBC) method for DFTB to model periodicity [15] and they used objective molecular dynamics (OMD) [16]. Difference in our results can mostly be accounted for by the differences between our computational methods and parametrizations. The detailed process of the parametrization is described in a section 3.

Parametrization reduces the amount of needed computational capacity. This is a

significant merit of DFTB. Heavy *ab initio* methods yield accurate results, but they need much resources. Without access to these resources it is not possible to execute this kind of computations. In the contrary, the computations of this study were run on a desktop computer and there was no need for large computational capacity.

In this study the computations contain three parts: in-plane stretching, in-plane shearing and bending. Stretching gives the starting point to see how DFTB models electronic band structures and are the results reliable. Shear deformations show interesting splitting in band structures. This ensures that we can obtain same kind of a behavior as in full DFT study about shearing by Sa *et al.* [17]. The bending was not done only in ac- and zz-directions but also in intermediate directions which shows well the relation between bending and shearing. In this study phosphorene sheet is only slightly bent resulting into large radii of curvature. The used computation package was Hotbit [18, 19] which is a free DFTB calculator package for Atomic Simulation Environment (ASE) [20].

2 Theoretical background

As in all atomistic simulations, the starting point lies in quantum many-body problem. This problem cannot be solved explicitly, because the number of interactions is just too large. Fortunately there are several different ways to simplify it. For example, one can use different flavors of perturbation theory, Green's functions or density-functional theory. Density-functional theory (DFT) is one of the most popular methods among material physics and quantum chemistry.

DFT was first presented in 1964 by Hohenberg and Kohn [21]. It is an *ab initio* method, which makes it accurate. On the other hand, it is still computationally demanding although lighter than Hartree-Fock methods. It cannot be used for large systems. In these cases one needs to make further approximations. One method is to introduce tight-binding approximation to DFT. The theory is called density-functional tight-binding (DFTB). Tight-binding is related to linear combinations of atomic orbitals (LCAO), which is presented in detail by Slater and Koster in 1954 [22].

In order to reduce needed computational effort, DFTB uses some preset information about the system such as energy levels of the energetically highest orbitals and repulsive behavior between the atoms. This information is included in the parametrization, which determines the accuracy of the method. The parameters emerge from the energetics when the total energy of the system is divided to different terms. It's usual to use information about simple systems, calculated with DFT, helping to fit the parameters. It is also possible to use experimental data in parametrization. [18]

In this section the theoretical basis of the density-functional tight-binding is presented. First the original density-functional theory is considered. It forms a basis for DFTB. Then Kohn-Sham approach to quantum many-body problem is introduced. This helps to handle the energies and divide them to three parts: repulsive energy term, Coulombic energy term and band structure term. The suitable representation is introduced for every energy term. While considering the band structure term, the actual tight-binding or LCAO is included. Finally the Mulliken population analysis

is introduced. After showing the machinery of the DFTB the focus is changed to periodicity. There the revised periodic boundary conditions (RPBC) approach is adopted.

2.1 Starting from density-functional theory

The starting point for derivation is the many-body Hamiltonian. It consists of four parts: kinetic energy of the electrons, external potential, electron-electron interaction and nuclei-nuclei interaction (sometimes called ion-ion interaction) [23]. Sometimes the latter part is considered as a constant for the system. This way it would just change the ground state of the energy, but now this is not a case. Positions of the nuclei determine the total energy of the system. Mathematically this is $E = E(\vec{R}_1,\vec{R}_2,\ldots)$. Hamiltonian in atomic units is

$$\hat{H} \;=\; -\frac{1}{2}\sum_i \nabla_i^2 \;+\; \sum_i V_{ext}(\vec{r_i}) \;+\; \frac{1}{2}\sum_{i\neq j}\frac{1}{|\vec{r_i} \;-\; \vec{r_j}|} \;+\; \frac{1}{2}\sum_{i\neq j}\frac{1}{|\vec{R}_i \;-\; \vec{R}_j|}. \qquad (1)$$

In order to construct the DFT formalism two theorems presented by Hohenberg and Kohn are needed [21]. The first theorem states that the ground state particle density determines external potential uniquely. This means that there is a clear one-to-one relation between the particle density and the potential where the particles exist, which leads to determination of the hamiltonian. If the hamiltonian is determined by the density, then wavefunctions are also determined by the density. In the end this states that the system can be fully presented by particle density. [23, pp.122]

The second theorem states that there is a functional for the energy $E[n(\vec{r})]$, which is determined by the external potential. Furthermore for every potential there exists a density minimizing the energy functional. This density is the ground state particle density n_0.

The proof for the first one is straghtforward. It is presented in the original paper of Hohenberg and Kohn and it proceeds with *reductio ad absurdum* [21]. The system has two different states Ψ_1 and Ψ_2, which are the ground states of the corresponding hamiltonian

$$E_1 \;=\; \langle\Psi_1|\hat{H}_1|\Psi_1\rangle \;<\; \langle\Psi_2|\hat{H}_1|\Psi_2\rangle. \qquad (2)$$

Only difference between H_1 and H_2 is the external potential. Therefore one can write

$$\langle\Psi_2|\hat{H}_1|\Psi_2\rangle \;=\; \langle\Psi_2|\hat{H}_2|\Psi_2\rangle \;+\; \langle\Psi_2|\hat{H}_1-\hat{H}_2|\Psi_2\rangle \tag{3}$$

$$\;=\; E_2 \;+\; \int \mathrm{d}\vec{r}\,[V_{ext,1}(\vec{r})-V_{ext,2}(\vec{r})]\,n_0(\vec{r}) \tag{4}$$

from which follows

$$E_1 \;<\; E_2 \;+\; \int \mathrm{d}\vec{r}\,[V_{ext,1}(\vec{r})-V_{ext,2}(\vec{r})]\,n_0(\vec{r}). \tag{5}$$

The same procedure can be executed starting with $\langle\Psi_1|\hat{H}_2|\Psi_1\rangle$. This yields the same equation with indices interchanged,

$$E_2 \;<\; E_1 \;+\; \int \mathrm{d}\vec{r}\,[V_{ext,2}(\vec{r})-V_{ext,1}(\vec{r})]\,n_0(\vec{r}). \tag{6}$$

If the ground state densities are identical, then the summation of these two equations would give $E_1 + E_2 < E_2 + E1$. This contradiction shows that for the different potentials there have to be an unique ground state density describing the system.

The second theorem shows that potentials correspond to ground state wavefunctions. The proof for this one too is simple. The energy functional for the system is

$$E[n] \;=\; T[n] \;+\; E_{ee}[n] \;+\; \int \mathrm{d}\vec{r}V_{ext}(\vec{r})n(\vec{r}) \;+\; E_{nn}. \tag{7}$$

In the equation (7) the kinetic energy and the electron-electron interaction energy are universal for all systems. They can be included into Hohenberg-Kohn functional

$$F_{HK}[n] \;=\; T[n] \;+\; E_{ee}[n]. \tag{8}$$

This is substituted into the equation (7) and it yields

$$E[n] \;=\; F_{HK}[n] \;+\; \int \mathrm{d}\vec{r}V_{ext}(\vec{r})n(\vec{r}) \;+\; E_{nn}. \tag{9}$$

Two potentials are different if $v_1 \;\neq\; v_2 + C$, where C is a constant. Two different potentials should yield different wavefunctions, which differ more than just by a phase factor. Let's assume that there are two potentials that fulfill the previous inequality but they still yield the same wavefunction and electron density. This also

states that Hamiltonian operators are otherwise the same but the potential terms are not. Then the difference between two state energies are

$$\hat{H}_1\Psi \ - \ \hat{H}_2\Psi \ = \ (\hat{V}_1 \ - \ \hat{V}_2)\Psi \ = \ (E_1 \ - \ E_2)\Psi \ = \ C\Psi \ . \tag{10}$$

The difference between two energies is always some other constant energy value. This creates a contradiction between our starting assumption, which means that two different potentials cannot yield same wavefunction. This proves that there is one-to-one relation between a potential and a wavefunction. Now it has been proved that the potential defines wavefunction which can be presented with electron density.

2.2 Moving towards density-functional tight-binding

After creating the basis, Kohn-Sham DFT needs to be considered. The essence of the Kohn-Sham approach to quantum many-body problem is to assume that the ground state of the interacting system is identical to suitable non-interacting system. Then so-called exchange-correlation term is introduced to DFT. This term is used to handle many-body interactions so that they are separated from the simpler non-interacting terms. [23, pp.135-136]

The derivation of DFTB follows reference [18]. The energy of the system can be written as [18]

$$E \ = \ T \ + \ E_{ext} \ + \ E_{ee} + \ E_{nn}, \tag{11}$$

which corresponds the Hamiltonian operator introduced in the equation (1). Here the equation (11) contains many interaction terms. In order to simplify the situation and hide the electron-electron interactions, exchange-correlation energy E_{xc} is used. It is represented as $E_{xc} = T - T_s + E_{ee} - E_H$ [18], where E_H is so-called Hartree energy and T_s is the kinetic energy of the electron in non-interacting system. This is a Kohn-Sham expression for the energy functional [23] as described earlier. E_{xc} is substituted to equation (11) and

$$E[n(\vec{r})] \ = \ T_s \ + \ E_{ext} \ + \ E_H \ + \ E_{xc} \ + \ E_{nn} \ . \tag{12}$$

According to Koskinen and Mäkinen this can be written explicitly as

$$E[n] \;=\; \sum_a f_a \langle \Psi_a | \left(-\frac{1}{2}\nabla^2 + V_{ext} + \frac{1}{2}\int \frac{n(\vec{r'})}{|\vec{r'} - \vec{r}|} \mathrm{d}\vec{r'} \right) |\Psi_a\rangle + E_{xc}[n] + E_{nn} \;, \quad (13)$$

where f_a is the occupation of the state [18]. This occupation follows Pauli's exclusion principle. Every state can have maximum of two electrons with opposite spins. This means that f_a belongs to an interval [0,2]. It has to be noted that we are not considering spin explicitly but the Pauli exclusion principle has to be followed, because electrons are fermions.

Next initial density $n_0(\vec{r})$ is considered. It is not an actual ground state density but it contains the atomic densities of free atoms. As one can guess it won't minimize the energy, because it is an artificial starting point. Adding small fluctuation $\delta n_0(\vec{r})$ to this density the real ground state density is obtained. Then $E[n]$ is expanded using this density information and then [18]

$$\begin{aligned} E[\delta n] \;\approx\; & \sum_a f_a \langle \Psi_a | -\frac{1}{2}\nabla^2 + V_{ext} + V_H[n_0] + V_{xc}[n_0] | \Psi_a \rangle \\ & + \frac{1}{2}\int\int \mathrm{d}\vec{r}\mathrm{d}\vec{r'} \left(\frac{\delta^2 E_{xc}[n_0]}{\delta n \delta n'} + \frac{1}{|\vec{r} - \vec{r'}|} \right) \delta n \delta n' \\ & - \frac{1}{2}\int \mathrm{d}\vec{r} V_H[n_0](\vec{r}) n_0(\vec{r}) + E_{xc}[n_0] + E_{nn} - \int \mathrm{d}\vec{r} V_{xc}[n_0](\vec{r}) n_0(\vec{r}). \end{aligned} \quad (14)$$

In equation (14) the first line is called the band structure energy E_{BS}. The second line contains charge fluctuation, Coulomb interaction and exchange correlation terms. It's denoted by E_{coul}. The third one is repulsive energy because of nuclei-nuclei interaction and its notation is E_{rep} [18]. Separately

$$E_{BS} = \sum_a f_a \langle \Psi_a | -\frac{1}{2}\nabla^2 + V_{ext} + V_H[n_0] + V_{xc}[n_0] | \Psi_a \rangle \;, \quad (15)$$

$$E_{coul} = \frac{1}{2}\int\int \mathrm{d}\vec{r}\mathrm{d}\vec{r'} \left(\frac{\delta^2 E_{xc}[n_0]}{\delta n \delta n'} + \frac{1}{|\vec{r} - \vec{r'}|} \right) \delta n \delta n' \quad (16)$$

and

$$E_{rep} = -\frac{1}{2}\int \mathrm{d}\vec{r} V_H[n_0](\vec{r}) n_0(\vec{r}) + E_{xc}[n_0] + E_{nn} - \int \mathrm{d}\vec{r} V_{xc}[n_0](\vec{r}) n_0(\vec{r}) \;. \quad (17)$$

The repulsive energy term is the place where everything difficult to calculate is hidden. This term is not calculated explicitly in DFTB, but it is treated with parametrization. Simple pair interactions can be calculated relatively easily using for example full DFT or some other sophisticated method. The acquired information is then used to fit repulsive potential to describe the system. During the parametrization an approximate solution for the repulsive term is created and it is adjusted according to the high-level calculations about the simple systems. It is also possible to use for example experimental data about system in order to describe repulsion properly. [18]

The first energy term to regard is the charge fluctuation term E_{coul}. In its current form it is not useful. It needs some modification. The process follows the reference [18]. The energy of an atom can be expressed using Δq extra electrons as [24, pp. 88-91]

$$\begin{aligned} E(\Delta q) &\approx E_0 + \left(\frac{\partial E}{\partial \Delta q}\right)\Delta q + \frac{1}{2}\left(\frac{\partial^2 E}{\partial \Delta q^2}\right)\Delta q^2 \\ &= E_0 - \chi \Delta q + \frac{1}{2} U \Delta q^2. \end{aligned} \tag{18}$$

Here χ and U are electronegativity and Hubbard U. They are defined as

$$\chi \approx \frac{\mathrm{IE} + \mathrm{EA}}{2} \tag{19}$$

and

$$U \approx \mathrm{IE} - \mathrm{EA}. \tag{20}$$

IE is ionization energy and EA is electron affinity. These two values are known for different elements. This helps greatly the modification of E_{coul}.

Now the volume integral is divided into fractions for every atom I in a system. This makes it possible to handle the double integral in the E_{coul}. The integral is now denoted as

$$\int \mathrm{d}\vec{r} = \int_V = \sum_I \int_{V_I}. \tag{21}$$

Using this division the amount of extra electrons in atoms can be approximated. It is calculated by integrating over the small electron density fluctuation introduced in

equation (14). Follows that

$$\Delta q_I = \int_{V_I} \delta n(\vec{r}) \tag{22}$$

and the atomic contributions to $\delta n(\vec{r})$ are presented as

$$\delta n(\vec{r}) = \sum_I \Delta q_I \delta n_I(\vec{r}). \tag{23}$$

Here every $\delta n_I(\vec{r})$ is normalized [18]. The number of extra electrons is directly Δq_I because the derivation is done in atomic units. This means that $e = 1$. Otherwise Δq_I would be the charge caused by extra electrons and thus it would have to be divided by e.

Koskinen and Mäkinen show in their article [18] a handy method to solve the Coulombic energy term E_{coul} in parts using the relations derived above. The relation of $\delta n(\vec{r})$ is used to describe E_{coul} as a sum of atom pairs IJ. There are two cases: $I = J$ and $I \neq J$. In the case of $I = J$

$$\frac{1}{2}\Delta q_I^2 \int_{V_I}\int_{V_I}' \left(\frac{\delta^2 E_{xc}[n_0]}{\delta n \delta n'} + \frac{1}{|\vec{r} - \vec{r'}|} \right) \delta n_I \delta n_I'. \tag{24}$$

Now the equations (18) and (24) are compared. There is a clear similarity to the third term of the equation (18). So it is possible to use Hubbard U as an approximation for the integral in E_{coul} when $I = J$. [18]

The next case to consider is the situation when $I \neq J$. Following the reference [18], this inequality makes the exchange-correlation contributions to vanish. The integral changes to

$$\frac{1}{2}\Delta q_I \Delta q_J \int_{V_I}\int_{V_J}' \frac{\delta n_I \delta n_J'}{|\vec{r} - \vec{r'}|}. \tag{25}$$

Now a suitable description for $\delta n_I(\vec{r})$ is still not known. There is no straightforward solution for the integral, but with suitable assumptions it is solvable. Assuming $\delta n_I(\vec{r})$ to have a Gaussian profile it is possible continue [25]. This yields

$$\delta n_I(\vec{r}) = \frac{1}{(2\pi\sigma_I^2)^{2/3}} e^{-r^2/(2\sigma_I^2)}, \tag{26}$$

where

$$\sigma_I = \frac{\mathrm{FWHM}_I}{\sqrt{8\ln 2}}. \tag{27}$$

FWHM stands for full width half maximum. The equality in the equation (26) is substituted into equation (25). Then

$$\int_V \int_V' \frac{\delta n_I \delta n_J'}{|\vec{r} - \vec{r}'|} = \frac{\mathrm{erf}(C_{IJ} R_{IJ})}{R_{IJ}} \equiv \gamma_{IJ}(R_{IJ}), \tag{28}$$

where

$$C_{IJ} = \sqrt{\frac{4\mathrm{ln}2}{FWHM_I^2 + FWHM_J^2}}. \tag{29}$$

The behavior of the $\gamma(R_{IJ})$ is presented in the figure 1 of reference [18]. It behaves much like the $1/R_{IJ}$ when $R \gg FWHM$. The authors also point out that when $R \to 0$ then $\gamma \to C \cdot 2/\sqrt{\pi}$ [18]. This suggests that if $I = J$,

$$\gamma_{II}(R_{II} = 0) \;=\; \sqrt{\frac{8\mathrm{ln}2}{\pi}} \frac{1}{\mathrm{FWHM}_I} \tag{30}$$

and furthermore gives the approximate relation to FWHM

$$\mathrm{FWHM}_I = \sqrt{\frac{8\mathrm{ln}2}{\pi}} \frac{1}{U_I} \;\approx\; \frac{1.329}{U_I}. \tag{31}$$

Every element has their own Hubbard U, which now determines the whole charge transfer part. In the end these parts are included to the equation (16), which becomes

$$E_{coul} = \frac{1}{2} \sum_{IJ} \gamma_{IJ}(R_{IJ}) \Delta q_I \Delta q_J, \tag{32}$$

where

$$\gamma_{IJ}(R_{IJ}) = \begin{cases} U_I, & I = J \\ \frac{\mathrm{erf}(C_{IJ} R_{IJ})}{R_{IJ}}, & I \neq J. \end{cases} \tag{33}$$

2.3 LCAO approach is adopted

As mentioned in earlier sections while using tight-binding approximation, electrons can be thought to belong to certain nuclei. This means that their wavefunctions can be presented as a linear combination of the wavefunctions centered on a single nucleus. Mathematically this is described with a minimal local basis

$$\psi_a(\vec{r}) \;=\; \sum_{\mu} c_{\mu}^{a} \phi_{\mu}(\vec{r}). \tag{34}$$

This is just a linear combination of atomic orbitals (LCAO).

The atomic populations are calculated as [18]

$$q_I \;=\; \sum_{a} f_a \sum_{\mu\nu} \int_I \mathrm{d}\vec{r} \phi_{\mu}^{*}(\vec{r}) \phi_{\nu}(\vec{r}). \tag{35}$$

The overlap integral has a crucial role. If none of the orbitals belong to atom I, it becomes approximately zero. On the other hand if they both belong to same atom the integral is $\delta_{\mu\nu}$ (Kronecker delta) because of the orthonormality. If only μ belongs to atom I, the integral becomes

$$\int_I \mathrm{d}\vec{r} \phi_{\mu}^{*}(\vec{r}) \phi_{\nu}(\vec{r}) \;\approx\; \frac{1}{2} \int_I \mathrm{d}\vec{r} \phi_{\mu}^{*}(\vec{r}) \phi_{\nu}(\vec{r}) \;=\; \frac{1}{2} S_{\mu\nu}, \tag{36}$$

where $S_{\mu\nu}$ is an overlap integral of two orbitals. Using this the charge or the amount of electrons in the atom I can be calculated as [18]

$$q_I \;=\; \sum_{a} f_a \sum_{\mu \in I} \sum_{\nu} \frac{1}{2} \left(c_{\mu}^{a*} c_{\nu}^{a} \;+\; \text{c.c.} \right) S_{\mu\nu}, \tag{37}$$

where c.c. means complex conjugate. This is called Mulliken population analysis. It is discussed in the section 2.4 with more detail.

The energy equation (14) had originally three parts, which needed new representations. First the repulsive energy (17) was handled with a new repulsive potential, which is determined during the parametrization process. The Coulombic energy (16) is essentially determined by Hubbard U. The band structure energy E_{BS} in equation (15) is now constructed using the LCAO in equation (34). Then it is written as

$$E_{BS} \;=\; \sum_{a} f_a \sum_{\mu\nu} \langle \phi_{\mu} | H^0 | \phi_{\nu} \rangle \;=\; \sum_{a} f_a \sum_{\mu\nu} c_{\mu}^{*} c_{\nu}^{a} H_{\mu\nu}^{0}. \tag{38}$$

Interestingly the actual tight-binding approximation or LCAO is seen only in band structure energies. In the end all the parts of the total energy in the equation (14) are expressed in a suitable manner for DFTB. The new energy equation is

$$E \;=\; \sum_a f_a \sum_{\mu\nu} c_\mu^* c_\nu^a H_{\mu\nu}^0 \;+\; \frac{1}{2}\sum_{IJ} \gamma_{IJ}(R_{IJ})\Delta q_I \Delta q_J \;+\; \sum_{I<J} V_{rep}^{IJ}(R_{IJ}), \tag{39}$$

where

$$\gamma_{IJ}(R_{IJ}) = \begin{cases} U_I, & I = J \\ \frac{\mathrm{erf}(C_{IJ}R_{IJ})}{R_{IJ}}, & I \neq J. \end{cases} \tag{40}$$

2.3.1 Two-center approximation

While using tight-binding or LCAO approximation, there are some difficulties. There are difficult three-center integrals concerning overlapping orbitals which makes calculation extremely difficult [22]. Fortunately there are suitable approximations to make calculations much easier. One is to neglect three-center integrals and to concentrate on two-center ones [22]. Computational methods make it possible to calculate these relatively easily. Overlap integrals are calculated in simple cases and tabulated during the parametrization process. This way computing becomes less demanding and therefore calculations can be done with small technical resources.

Overlap integrals contain s, p and sometimes d orbitals. Every possible σ-, π- and δ-bonding case has to be tabulated. These are called Slater-Koster integrals and there are in total ten of them: $dd\sigma$, $dd\pi$, $dd\delta$, $pd\sigma$, $pd\pi$, $pp\sigma$, $pp\pi$, $sd\sigma$, $sp\sigma$ and $ss\sigma$ [18]. Now in the case of phosphorus s, p and d orbitals all are included. Even though d orbitals are now unoccupied, they play a key role for many properties of phosphorene.

Koskinen and Mäkinen present a clear example about the integration of overlap integrals using Slater-Koster transformations [18]. There are ten Slater-Koster integrals and 81 transformations in total. In the original paper of Slater and Koster they have presented transformations or matrix elements for different geometries [22].

2.3.2 Adding confinement to form pseudoatoms

Real orbitals of the free atoms are too diffuse to be used as such in tight-binding approximation [18]. They need to be constrained to a certain volume with a confinement potential V_{conf}. This potential is simply added to the Hamiltonian for every atom. The potential is spherically symmetric and it is presented generally as

$$V_{conf}(r) \;=\; \sum_{i=0}^{\infty} v_{2i} r^{2i}. \tag{41}$$

There are no odd terms included because of two requirements. The potential has to be symmetric in all directions and smooth when $r = 0$. Koskinen and Mäkinen choose to use only $v_2 r^2$ term [18]. This is reasonable because the first term is just a constant and higher order terms usually have only small influence. With this reasoning confinement potential is written as

$$V_{conf}(r) \;=\; \left(\frac{r}{r_0}\right)^2. \tag{42}$$

Here the parameter r_0 was introduced. This type of a quadratic choice has also been used by Porezag *et al.* for all types of atoms [26]. On the other hand the confinement potential is not restricted to only quadratic terms but it can also have other shapes [27].

2.4 Mulliken populations

The equation (37), in which the charge of atom I is calculated, is the so-called Mulliken population analysis. This method was first introduced by R. S. Mulliken in 1955 [28]. In this section this analysis method is considered more thoroughly than in the previous sections. István Mayer has presented this method well in his book in reference [29] so this description mostly follows it, even if some proofs are omitted.

The electron density is a starting point for the derivation. The density operator can be written as

$$\hat{\rho} \;=\; \sum_{i=1}^{N} \delta(\vec{r} \;-\; \vec{r_i}). \tag{43}$$

Here δ is Dirac's delta function, which means that one electron is highly localized to a single point in the space. Summing all these density peaks together the total electron density operator is acquired. The actual electron density is the expectation

value of this operator. While calculating this, the wavefunction is divided to position and spin parts as follows

$$\begin{aligned}\rho(\vec{r}) &= \langle\Psi|\hat{\rho}(\vec{r})|\Psi\rangle = \sum_{j=1}^{N}\langle\varphi_j(\vec{r}_1)\gamma(\sigma)|\delta(\vec{r}-\vec{r}_1)|\varphi_j(\vec{r}_1)\gamma(\sigma)\rangle \\ &= \sum_{j=1}^{N}|\varphi_j(\vec{r})|^2. \end{aligned} \tag{44}$$

The spin part $\gamma(\sigma)$ of the wavefunction is position-independent so they are not affected by $\delta(\vec{r}-\vec{r}_1)$. They are supposed to be orthonormal. The sum essentially needs only the position-dependent part of the wavefunction.

Now the electron density ρ is divided to different spin parts. Even though in equation (44) the spin parts disappear, they contribute to the density. It can be thought that originally the wavefunction Ψ contains orbitals a_i and b_i, which have opposite spin contributions. This can be written as

$$\Psi = \sum_i \left[a_i(\vec{r},\sigma_+) + b_i(\vec{r},\sigma_-)\right] = \sum_i \left[a_i(\vec{r})\gamma(\sigma_+) + b_i(\vec{r})\gamma(\sigma_-)\right], \tag{45}$$

where σ_+ and σ_- represent opposite spins. Orthonormality is of course preserved. Using this idea Mayer continues to divide $\rho(\vec{r})$ in two parts with opposite spins [29, pp.228]. This yields

$$\rho(\vec{r}) = \sum_{j=1}^{n_a}|a_j(\vec{r})|^2 + \sum_{j=1}^{n_b}|b_j(\vec{r})|^2. \tag{46}$$

Next the LCAO is used, which means that $a_j(\vec{r})$ and $b_j(\vec{r})$ are replaced with same type of an expansion as in equation (34). When this is done,

$$\rho(\vec{r}) = \sum_{j=1}^{n_a}\sum_{\nu=1}^{m} a_\nu^{j*}\chi_\nu^*(\vec{r})\sum_{\mu=1}^{m} a_\mu^j\chi_\mu(\vec{r}) + \sum_{j=1}^{n_b}\sum_{\nu=1}^{m} b_\nu^{j*}\chi_\nu^*(\vec{r})\sum_{\mu=1}^{m} b_\mu^j\chi_\mu(\vec{r}). \tag{47}$$

This is not a clear way to write the equation (47). In order to tidy it up Mayer [29, pp.229] uses the elements of so called P-matrices. He defines them as

$$\mathbf{P}^l = \sum_{i=1}^{n_l}\mathbf{a}^i\mathbf{a}^{i\dagger}. \tag{48}$$

In this case bold font means that the variable is a matrix. Using these matrix elements, equation (47) becomes

$$\begin{aligned}\rho(\vec{r}) &= \sum_{\mu,\nu=1}^{m} (P^a_{\mu\nu} + P^b_{\mu\nu})\chi^*_\nu(\vec{r})\chi_\nu(\vec{r}) \\ &= \sum_{\mu,\nu=1}^{m} D_{\mu\nu}\chi^*_\nu(\vec{r})\chi_\nu(\vec{r}),\end{aligned} \tag{49}$$

where $D_{\mu\nu}$ is the element of the ‘‘spinless density matrix’’ [29, pp.229]:

$$\mathbf{D} = \mathbf{P}^a + \mathbf{P}^b. \tag{50}$$

Using the matrix (50) it is possible to calculate the total number of electrons N. This is done by multiplying it with the overlap matrix $\mathbf{S}$ and then tracing it [29, pp.230]. Matrix $\mathbf{S}$ contains the same Slater-Koster integrals that were introduced in two-center approximation. The number of electrons becomes

$$N = \mathrm{Tr}(\mathbf{DS}) = \sum_{\mu}^{m}(\mathbf{DS})_{\mu\mu} = \sum_{\mu,\nu=1}^{m} D_{\mu\nu}S_{\mu\nu}. \tag{51}$$

It is usually interesting to know the population of the certain orbital type. In that case ‘‘Mulliken’s gross orbital population’’ q_μ is needed. Here μ corresponds an orbital and [29, pp.230]

$$q_\mu = (\mathbf{DS})_{\mu\mu} = \sum_{\nu=1}^{m} D_{\mu\nu}S_{\nu\mu}. \tag{52}$$

If all orbitals μ, that belong to a certain atom A, are summed, the gross atomic population is

$$Q_A = \sum_{\mu\in A} q_\mu = \sum_{\mu\in A}(\mathbf{DS})_{\mu\mu} = \sum_{\mu\in A}\sum_{\nu=1}^{m} D_{\mu\nu}S_{\nu\mu}. \tag{53}$$

This is the total population of the atom A. In this study the gross orbital population q_μ for the single atom was used. This was especially important while bending the phosphorene sheet, because this kind of an analysis makes it possible to observe how the populations change in inner and outer parts of the sheet.

2.5 Revised Periodic Boundary Conditions (RPBC)

In this study the periodicity has a central role. In general many structures that are studied in solid state physics are periodic. This way computations are much easier, because it is enough to simulate a single unit cell with suitable boundary conditions. As described in the introduction, the unit cell of the phosphorene contains four atoms and it is periodic in in-plane directions. The method to handle periodicity of the structure was RPBC [15]. This approach is used by Hotbit calculator. Basically the theory is a new form of Bloch's theorem. It represents symmetries as operators.

Usually Bloch's theorem is written as [30, pp. 163-164]

$$\psi_{a\vec{k}}(\vec{r}-\vec{T}) \;=\; e^{-i\vec{k}\cdot\vec{T}}\psi_{a\vec{k}}(\vec{r}). \tag{54}$$

This means that in an initial unit cell lies a point $\vec{r}$ and a translation $\vec{T}$ is added to it. Translation moves the point in the periodic direction. This causes the original wavefunction to be multiplied with additional phase factor. In the end the wavefunction is the same as in position $\vec{r}$ but its phase is changing due the periodicity

From now on the derivation follows the references [15] and [31]. Next Kit *et al.* introduce another way to represent this transformation [15]. Translation can be denoted with operator $\tau^n\vec{r} = \vec{r} + \vec{T_n}$ and corresponding inverse transformation $\tau^{-n}\vec{r} = \vec{r} + \vec{T_{-n}} = \vec{r} - \vec{T_n}$. Then they use action $\hat{D}(\tau^n)$ to describe the Bloch's theorem as [15]

$$\hat{D}(\tau^n)\psi_{a\vec{k}}(\vec{r}) = \psi_{a\vec{k}}(\tau^{-n}\vec{r}) = e^{-i\vec{k}\cdot\vec{T}_n}\psi_{a\vec{k}}(\vec{r}). \tag{55}$$

In order to proceed into actual revised Bloch's theorem authors point out that the electrons within a potential should be invariant in a general symmetry operation $\vec{r'} = S^n\vec{r}$. In other words the potential is symmetric (invariant in symmetry operation) as [15, 31]

$$\hat{D}(S^n)V(\vec{r}) = V(S^{-n}\vec{r}) = V(\vec{r}). \tag{56}$$

The revised Bloch's theorem works with any symmetries not just with translations. Next they use a set of commuting symmetry operations $S_i^{n_i}$ by notation $S^{\vec{n}} \equiv S_1^{n_1}S_2^{n_2}\ldots$. If symmetry operation is used for wavefunction, one gets

$$\hat{D}(S^{\vec{n}})\psi_{a\kappa}(\vec{r}) = \psi_{a\kappa}(S^{-\vec{n}}\vec{r}) = e^{-i\kappa\cdot\vec{n}}\psi_{a\kappa}(\vec{r}). \tag{57}$$

They generalized $\vec{k}$ by using κ [15, 31]. The vector $\vec{n}$ is just a collection of integers that tell the number of corresponding symmetry operations $S_i^{n_i}$. Symmetry operations $\hat{D}(S^{\vec{n}})$ commute with each other and with Hamiltonian [15]. Because of the symmetry, if the operation is done several times, at some point it returns to its original state. This is represented as

$$\hat{D}(S^{\vec{M}}) = \hat{D}(S^{\vec{M}_1} S^{\vec{M}_2} \ldots) = 1 \tag{58}$$

and as before with $\vec{n}$ now $\vec{M} = (M_1' M_2' \ldots)$. On the other hand now $M_j' = 0$ or M_j. Here M_j is the number, which leads the operations back to the original system.

Following the original derivation next the unitarity of the symmetry operation is needed. In the reference [32, pp. 16-17] Rose points out that unitary operator can be represented uniquely using exponent of the Hermitian operator. This yields

$$\hat{D}(S^{\vec{n}}) = e^{-i\hat{\kappa}\cdot\vec{n}}, \tag{59}$$

which is essentially a constant. These leads to consider an eigenvalue problem

$$\hat{D}(S^{\vec{n}})|\psi\rangle = e^{-i\hat{\kappa}\cdot\vec{n}}|\psi\rangle = C_{\vec{n}}|\psi\rangle. \tag{60}$$

Here $C_{\vec{n}}$ is a constant. It is convenient to operate equation (60) from the left with $\langle\kappa|$, which leads to κ-representation

$$\langle\kappa|\hat{D}(S^{\vec{n}})|\psi\rangle = \langle\kappa|e^{-i\hat{\kappa}\cdot\vec{n}}|\psi\rangle = e^{-i\kappa\cdot\vec{n}}\psi(\kappa) = C_{\vec{n}}\psi(\kappa). \tag{61}$$

Next the eigenvalue equation (60) is operated from left with $\langle\vec{r}|$. The aim is to form position representation of ψ same way as its κ representation was formed. In that case

$$\langle\vec{r}|\hat{D}(S^{\vec{n}})|\psi\rangle = \langle S^{-\vec{n}}\vec{r}|\psi\rangle = e^{-i\kappa\cdot\vec{n}}\langle\vec{r}|\psi\rangle \tag{62}$$

and then in position presentation

$$\hat{D}(S^{\vec{n}})\psi(\vec{r}) = \psi(S^{-\vec{n}}\vec{r}) = e^{-i\kappa\cdot\vec{n}}\psi(\vec{r}). \tag{63}$$

Next step in the original derivation [15] is to use the cyclic conditions from equation (58). This leads to restrict the values of κ which is seen as

$$e^{i\kappa_j M_j} = 1 = e^{i2\pi m_j} \tag{64}$$

and then

$$\kappa = 2\pi \left(\frac{m_1}{M_1}, \frac{m_2}{M_2}, \ldots \right), \tag{65}$$

where $m_j = 0, 1, 2, \ldots M_{j-1}$. In the end κ is a good quantum number and revised Bloch's theorem is proved [15]. This representation of Bloch's theorem makes it possible to handle easily several different symmetries such as planes, tubes and spheres just by using suitable operators. These geometries are implemented into the Hotbit and all of them can be found in references [15] and [19].

3 Parametrization for DFTB and the basic properties of phosphorene

The parametrization process has two main parameter types to determine. The first type is electronic parameters and the second type is repulsive energy parameters [33]. Some of these parameters are acquired directly from the computations. On the other hand repulsive energy parameters are adjusted mostly by hand. Theory behind the parameters is described in the theory part. Here the parameter determination process and actual parameters are presented. The parameters are listed in table 1.

The first electronic parameters are acquired directly in the beginning of the process. They are calculated by Hotbit according to its pre-set information about different atoms. They are the energies of the highest occupied orbitals ($3s$ and $3p$), Hubbard U and full width half maximum (FWHM) of the Gaussian profile of the Coulombic interaction term. After these we added the energy of the $3d$ orbitals which are unoccupied. This value was adjusted several times. Most importantly it affects to the size of the band gap.

After determining the parameters to represent individual atoms, the task was to define the orbital overlap into the Slater-Koster tables. Here the parameter r_0 was set. As explained in the theory part r_0 is used to create spacially restricted pseudoatoms and it is usually kept about twice the size of the covalent bond length (r_{cov}) [18, 26]. Length of the covalent bond is acquired directly from the calculations so only the multiplier is needed.

The third step is to find suitable repulsive potential between the atoms. First some simple structures with constant bond length were scaled using full DFT and the repulsive forces were measured. This produced several data points where force was presented as a function of bond length. The structures were dimer, white phosphorus (tetrahedron), red phosphorus (chain of tetrahedrons), and black phosphorus. Next task was a curve fitting to these data points. Giving them suitable weights the position and the form of the curve was adjusted. The smoothness of the curve was controlled with parameter s. The distance where the repulsion became zero was

determined by r_{cut} parameter. The repulsive force curve was used to integrate the repulsive energy curve. These are presented in the figure 2.

In the figure 2 dimer has two different values to weight. The literature value for the bond length was set to 1.895 Å and the repulsion was calculated by Hotbit. The result was weighted with w_{dimer}. Another parameter for dimer was w_{dimer_curve}. It weights the repulsion data points formed by stretching the bond. The repulsion in stretching was calculated with DFT.

Finding the parameters was done by repeating the same steps several times. First electronic parameters were set and then repulsive potential was formed. After this the unit cell was optimized and some basic properties were calculated. They were compared to the literature values. The properties were the dimensions of the unit cell, bond lengths, Young's moduli, shear moduli, Poisson ratios, bending moduli, band gap and the overall band structure. After the comparison parameters were adjusted and the process was repeated.

Table 1. Only ϵ_{3s}, ϵ_{3p}, U and FWHM were acquired directly from the computations. Here s determines the smoothness of the repulsion curve. Weights of different data points are w_i. Bohr radius is r_{Bohr}

Parameters	Values
ϵ_{3s}	-0.512163 eV
ϵ_{3p}	-0.206132 eV
ϵ_{3d}	0.262 eV
U	0.293863 Ha
FWHM	4.52019 r_{Bohr}
r_0	$1.873 \cdot\ r_{cov}$
r_{cut}	2.58 Å
s	5.9
w_{dimer}	0.6
w_{dimer_curve}	1.6
w_{WP}	0.7
w_{RP}	0.6
w_{BP}	1.6

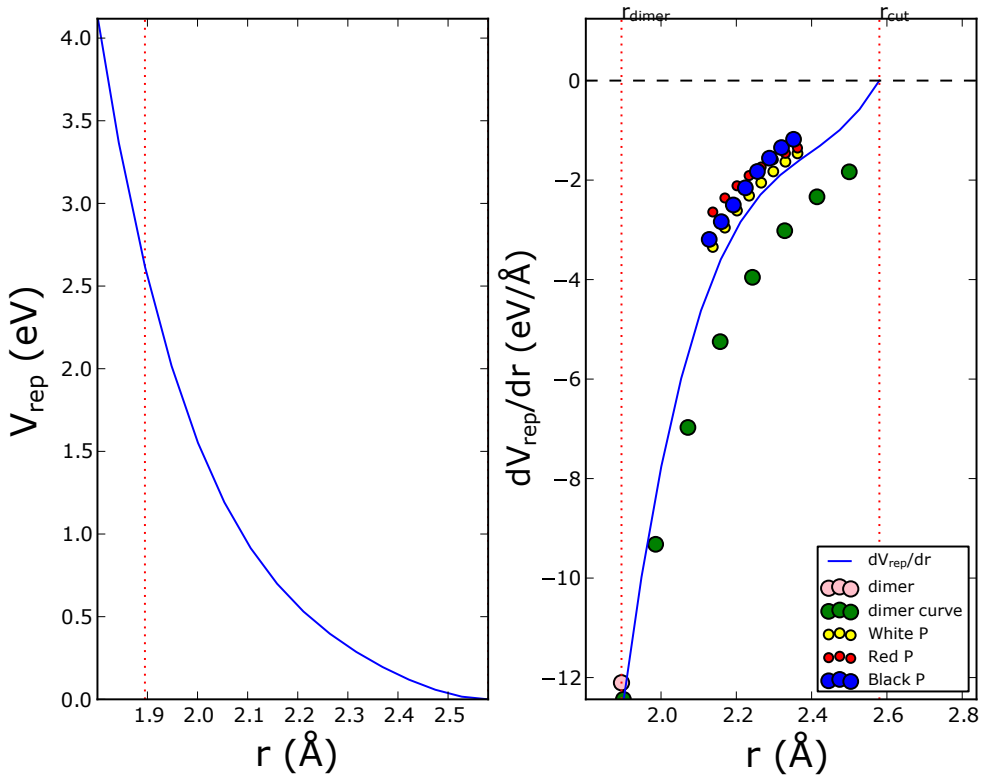

Figure 2. Right side presents the repulsive forces. The datapoints are acquired from scaling of the corresponding structures with constant bond lengths using DFT. On the left there is a repulsive energy curve which is integrated from the repulsive force curve.

Gaus *et al.* have also formed a DFTB parametrization for phosphorus [33]. Our electronic parameters are in agreement. It has to be noted that ϵ_{3d} differs significantly, but this is not a concern. Gaus *et al.* have done parametrization for phosphorus in general case, but ours is designed especially for phosphorene. Also our other parameters have effects that overlap with the ones of ϵ_{3d}. The parametrization is always a compromise between different properties to model.

The parametrization is done so that it could be used to simulate phosphorene as well as possible in both mechanical and electronic cases. On the other hand the broadness causes some errors. The most significant one is the direct band gap. The gap should be essentially direct in Γ point but because of the parametrization the peak in the Γ-Y path is slightly higher than the peak in Γ. In this study we focus on the direct band gap in Γ. The other phenomena are observed qualitatively in

comparison to this. The initial band structure can be seen in the figure 4a).

The properties that were acquired from the final parametrization are listed in the tables 2, 3 and 4 with reference results from other studies. These are the same properties which were described earlier. We studied just a single layer of phosphorene, so the z dimension of the unit cell is not relevant. DFTB cannot be used to determine the z dimension of the unit if there are no interactions in that direction. Furthermore the interaction between two planes are van der Waals interactions, which would need a different parametrization [18].

In table 2 there are some reference values for the physical dimensions of the phosphorene. There are some clear trends in the values. Our parametrization yields results in the correct scale but they don't fully agree with previous studies. This happens, because we emphasized the elastic and electronic properties of the phosphorene in the parametrization. Bond angle α is large and β is small compared to previous studies. Also bond lengths and unit cell dimensions differ as seen in the table 2. If these dimensions would be perfect the problem is that some more important elastic or electronic properties, such as the size of the band gap, would be flawed.

The most suitable reference for the elastic properties is the paper written by Verma *et al.* [14]. They used objective molecular dynamics (OMD) [16], which is related to revised periodic boundary conditions (RPBC) [15] used in this study. They have computed the bending moduli, Young moduli, shear moduli and Poisson ratios in every direction in the plain of the phosphorene. Also some other results about elastic properties were used as a reference. These are presented in the table 3. Results are in a good agreement. There are no such problems as with bond lengths and angles. Interestingly shear moduli of this study differ little bit depending on the direction but values computed by Verma *et al.* do not differ [14].

We computed that the direct band gap was 1.872 eV. Earlier it was mentioned that the band gap of phosphorene is determined to be up to about 2.0 eV [5] so the result is reasonable. It is worth mentioning that the band gap of single layer phosphorene is always larger than the band gap of the bulk black phosphorus, which is around 0.3 eV [5, 6, 34]. There are also numerous other studies where the band gap has been determined computationally. Some of them are listed in the table 4. Most of the DFT methods seem to underestimate the size of the band gap. They are nearly always considerably smaller than experimental results. Despite this variation

in different studies, the band gap yielded by DFTB seems to agree with reference results in the table 4.

Table 2. Here are listed the bond lengths, bond angles and the unit cell dimensions from the different references and from this study. Comparing these values it can be seen that the parametrization yields reasonable physical measures for the phosphorene.

Method	d_1 [Å]	d_2 [Å]	α [°]	β [°]	x [Å]	y [Å]
DFTB (this study)	2.220	2.236	98.903	101.309	3.374	4.236
DFT (PBE, PAW) [35]	2.22	2.26	95.9	104.1	3.298	4.627
DFT (GGA, PBE, DFT-D2)[36]	2.22	2.25	96.28	103.75	--	--
TB [37]	2.224	2.244	96.34	102.09	3.314	4.376
DFT [38]	2.24	2.28	96.00	103.51	3.32	4.58
DFT (PBE, HSE06)[6]	--	--	--	--	3.35	4.62

Table 3. Elastic properties of phosphorene have been studied in several papers. Here Y is Young's modulus, S shear modolus, σ Poisson's ratio and K is a bending modulus. Armchair direction is marked with ac and zigzag direction with zz.

Method	$Y[\frac{\mathrm{N}}{\mathrm{m}}]$	$S[\frac{\mathrm{N}}{\mathrm{m}}]$	σ	$K_{ac}[\cdot 10^{-18}\mathrm{J}]$
DFTB (this study)				
ac	32.135	38.258	0.267	0.444
zz	108.131	37.583	0.898	1.662
OMD [14]				
ac	33.3	31.2	0.31	0.524
zz	79.1	31.2	0.73	1.311
DFT (PBE, PAW) [35]				
ac	48.796	–	–	–
zz	184.094	–	–	–
VFFM* [39]				
ac	52.2	–	–	–
zz	85.4	–	–	–
analytic [40]				
ac	–	–	–	0.76949
zz	–	–	–	1.3781

*Valence Force Field Model

Table 4. Here are several values for the band gap of the phosphorene. The band gap vary depending on the used method. Especially many DFT studies have acquired relatively small band gaps compared to the experimental results.

Method	Band gap [eV]
DFTB (This study)	1.872
G_0W_0 [5]	2.0
G_1W_1 [5]	1.4
DFT (PBE, HSE06) [6]	1.0
DFT (GGA, PBE, DFT-D2)[36]	0.88
DFT [38]	1.51
DFT (PBE, GGA) [41]	0.91
DFT [42]	1.0
experimental [6]	1.45
experimental [8]	1.24
experimental [43]	2.05

4 Effects of elastic deformations to band structure

The main focus of the study was the electronic band structure of the phosphorene and its behavior during stretching, shearing and bending. All of these were done in both armchair and zigzag direction but bending was also done in other chiral directions. The curvature radii in these computations are large. The bending is much more modest than in nanotubes.

Electronic structure of phosphorene is sensitive to physical distortions which is seen as changes in the band structure. Although one has to note the weaknesses of the used DFTB method. As mentioned earlier, due to the parametrization the initial band gap is not direct as it should be. This is not a big concern because we measured only the direct band gap along the Γ point. With this kind of an approximate method the relative changes in the band structure are more important than the absolute ones.

Studying the band structure the orthorhombic lattice was used. The observed path in the Brillouin zone was S-X-Γ-Y-S. It is visualized in the figure 3. The notations follow the paper of the Setyawan and Curtarolo [44]. In the figures, where band structures are imaged, G corresponds to Γ. The zero level of the band structure plots is set around the Fermi level. In some cases computations did not yield exactly the same Fermi level but values varied. In order to make plots easier to analyze the zero energy level was set to be about 4.0 eV. This value was kept constant.

4.1 Stretching scales direct band gap

The band structures, that were computed during the stretching, are presented in the figure 4. When phosphorene was stretched or compressed its band gap started to change from direct to indirect and the size of the direct band gap changed. When compression in armchair direction increased, the band gap moved away from direct Γ. HOMO state was on the peak close to Y point in Γ-Y path and LUMO was still on Γ point. The change in HOMO state is so large that it can be verified even with

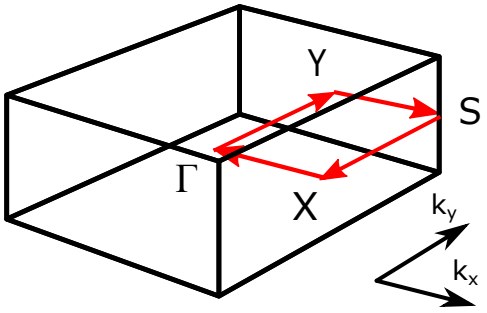

Figure 3. The path for observing the band structure within the orthorhombic Brillouin zone is similar to the one used in reference [44].

this parametrization. At the same time the actual band gap shrunk significantly as did the measured direct band gap. The phenomena are visible with just -6.87% strain. The same type of a phenomena was also observed by Peng, Wei and Copple [41] but they report that strain, which causes these changes, is between -12% and -8%. On the other hand, the actual stretching in ac-direction caused band gap to grow nearly as greatly as it shrunk in compression. Stretching kept band gap direct on the Γ point.

In zz-direction stretching caused band gap to change into an indirect one. In this case stretching in zz-direction made the lowest energy peak in the unoccupied states to move from Γ point towards the Y point. This happened when about 7% stretch was applied. This is the same behavior as reported by Peng, Wei and Copple [41]. Compression in zz-direction causes LUMO state to get closer to the HOMO. The band gap became smaller, but wether the transition from direct to indirect band gap happens is not clear with our parametrization.

The behavior of the direct band gap at Γ point of interest is visualized as a function of strain in figure 5. While studying the direct gap the maximum strain was $\pm 11\%$. Compression made the gap to shrink and stretching made it to grow in both directions. That's the only similarity. In armchair direction the gap behaves so that data points form a convex curve but in zigzag case they form concave curve as seen in figure 5. After about 6% stretching in zz-direction the gap began to shrink instead of growing. This behavior has been observed also by Peng, Wei and Copple for the real band gap [41] and by Qin *et al.* for the bulk phosphorus [34]. Later when the mulliken populations are studied one realizes that this is caused by the

changes in the orbital contributions of the LUMO state.

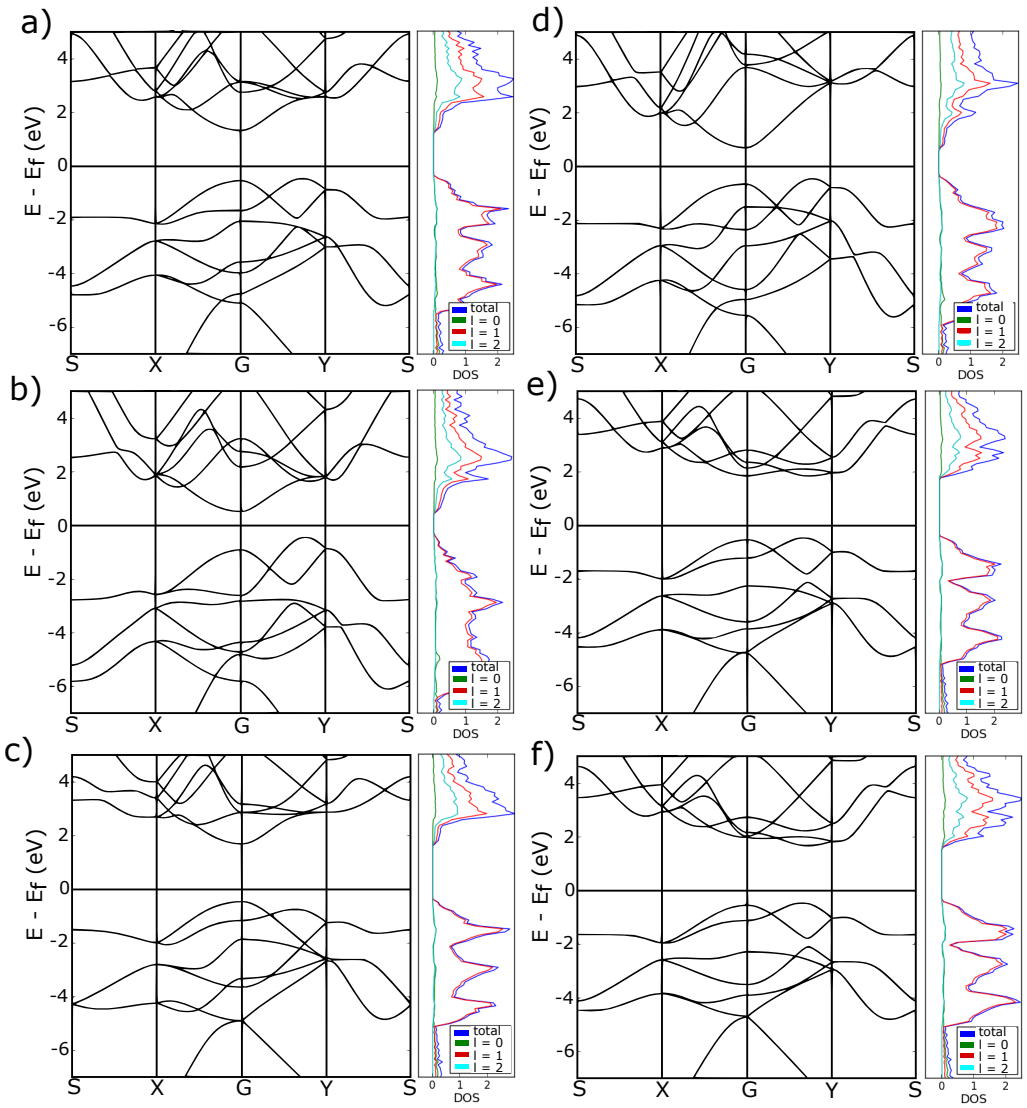

Figure 4. Stretching and compression cause significant changes in the band structure. In a) there is the initial band structure of the optimized structure, in b) unit has been compressed 6.87 % in ac-direction, in c) it has been stretched 6.88 % in ac-direction. The rest are for the zz-direction: d) sheet is compressed 6.87 %, e) sheet is stretched 5.50 % and f) stretching is 6.88 %. In zz-direction it is seen that between 5.50% and 6.88% stretching the band gap transforms into indirect one. Density of states (DOS) is imaged for angular quantum numbers $l = 0$, 1 and 2. Blue line is a total DOS.

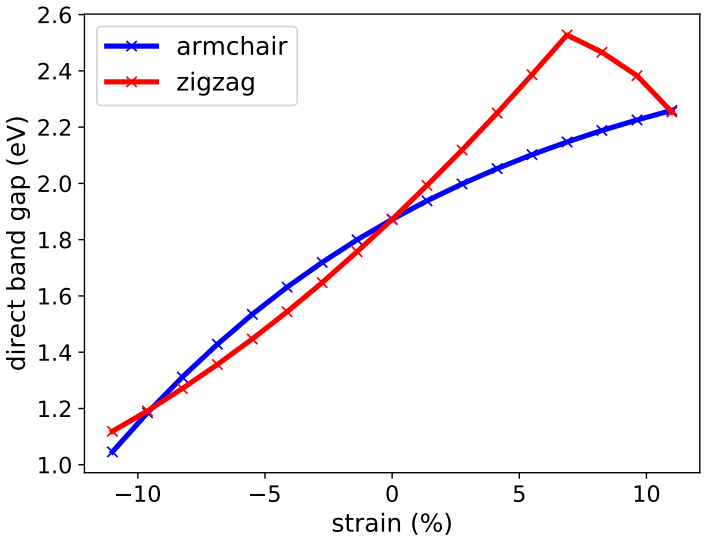

Figure 5. Stretching in ac- and zz-directions cause very different changes in the direct band gap. When strain is close to zero, both has overall the same trend about increase and decrease of the gap but the curving is not similar.

4.2 Shear causes band splitting

Shearing causes quite different changes into the band structure than stretching. Unlike in a previous section changes are mostly on the S-X and Y-S paths. Sa *et al.* have studied shearing of phosphorene in their paper [17]. They studied essentially the same paths as we did. They just use M instead S in the notations. They used DFT in the study so their results are much more reliable than ours. On the other hand the results are very similar. This shows that tight-binding approximation is capable to simulate phosphorene.

Shearing was done in both ac- and zz-directions. The direction means that the shear strain was applied along the corresponding axis. Maximum shear was 15% in both cases. Both directions caused similarly the splitting of the bands in both S-X and Y-S paths. Originally there has been a degeneracy within the bands but shearing made them to split. This is seen in both occupied and unoccupied bands. The splitting is clear already with a small shear. The band structures for ac are presented in the figure 6 and for zz in figure 7.

Taking into account the inaccuracy of the directness of the band it is not possible

to say for certain if shear changes the band gap from direct to indirect. The heights of the highest peaks along Γ-Y vary so little. Sa *et al.* report that the phophorene should turn into indirect band gap semiconductor when shear strain is larger than 4% [17]. Their band structure plots show that the lowest unoccupied band should change from Γ to the half way of their M-Y path. Our band structures do not show this kind of a phenomena. This is most likely caused by the used method. Unoccupied states are difficult to handle with as approximate method as DFTB.

Since the behavior of the real band gap is not computed correctly with DFTB, the direct band gap in Γ was studied. It is clear that the direct gap decreases when the shear is increased. In both ac- and zz-direction the behavior was smooth. This is presented in a figure 8.

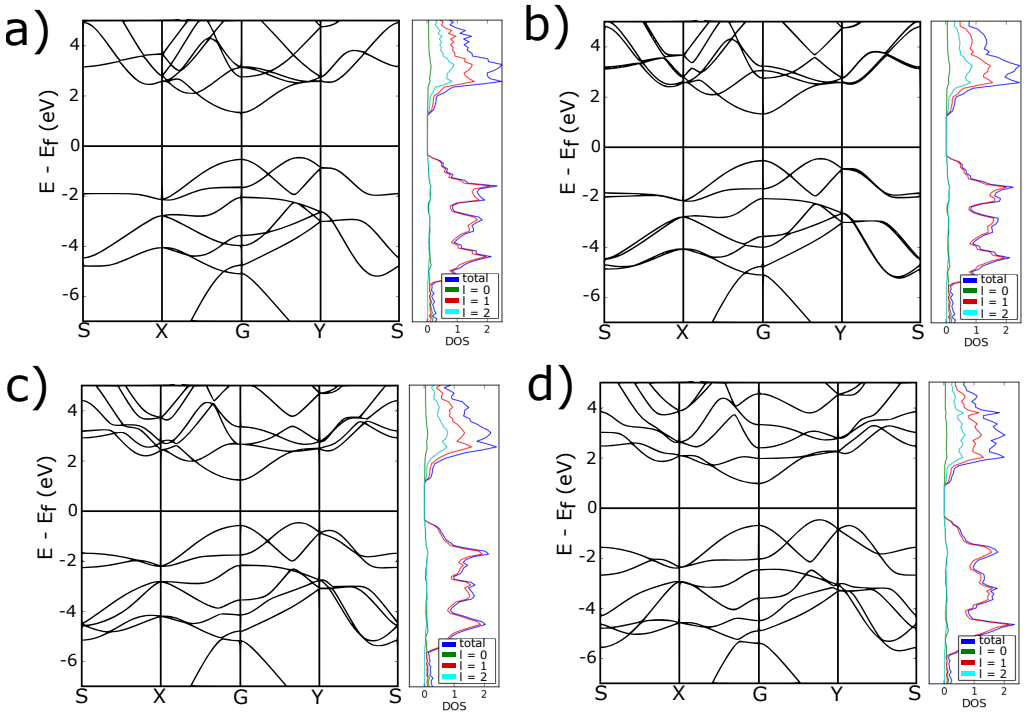

Figure 6. Figure a) is the initial band structure. In the rest shear is increased in the ac-direction: b) 1.87 %, c) 7.50 % and d) 15.00 %. Shearing in ac-direction causes splitting of the bands in the S-X and Y-S paths.

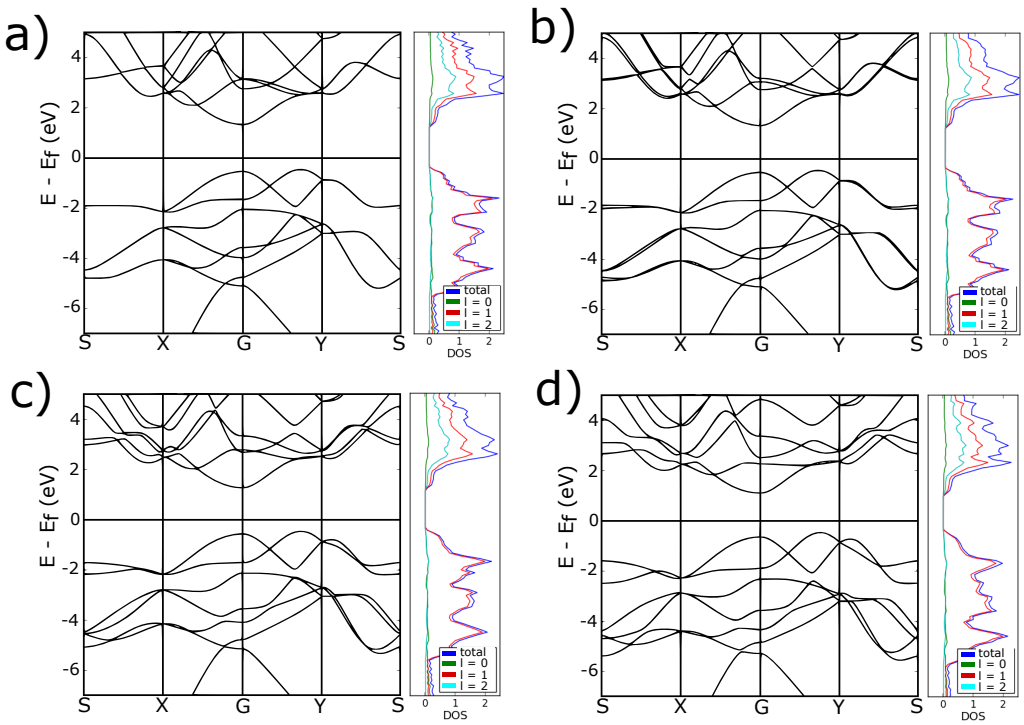

Figure 7. Figure a) is the initial band structure. In the rest shear is increased in the zz-direction: b) 1.87 %, c) 7.50 % and d) 15.00 %. Band splitting in the S-X and Y-S paths is also observed with shearing in zz-direction.

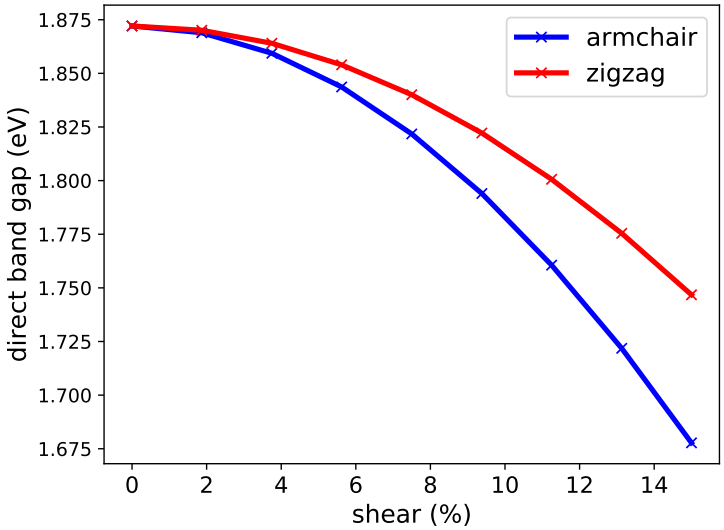

Figure 8. Shearing causes smooth changes on direct band gap. The direction for shearing means that it is done along that axis of the phosphorene unit cell.

4.3 Bending causes similar changes in band structure as shearing

Bending of phosphorene sheet is not done only in ac- and zz-directions but also in intermediate directions. Now if the sheet is bended in zz-direction, it means that the longitudinal axis, around which the sheet is bent, lies in ac-direction. In figure 1 this longitudinal axis is along y-axis. In the case of ac-bending this is vice versa. Longitudinal axis is along the zz-direction corresponding to x-axis in figure 1.

Bending causes interesting changes in the electronic band structure of phosphorene. Direct bending in both ac- and zz-directions causes splitting of the degenerate bands in Y-S path as seen in figures 9 and 10. The lines are clearly opening in the Y point. This splitting increases while the bending increases. The phenomenon is clearer in the zz-bending than in ac-bending. There are similarities to shear deformations. The difference in the magnitude of the splitting is partly explained by the anisotropic elastic porperties of phosphorene. There is also splitting directly at Y point which is not observed in shearing. In zz-bending in figure 10 lines are also diverging along greater distance between Y and S than only at Y point. This is also visible in shearing.

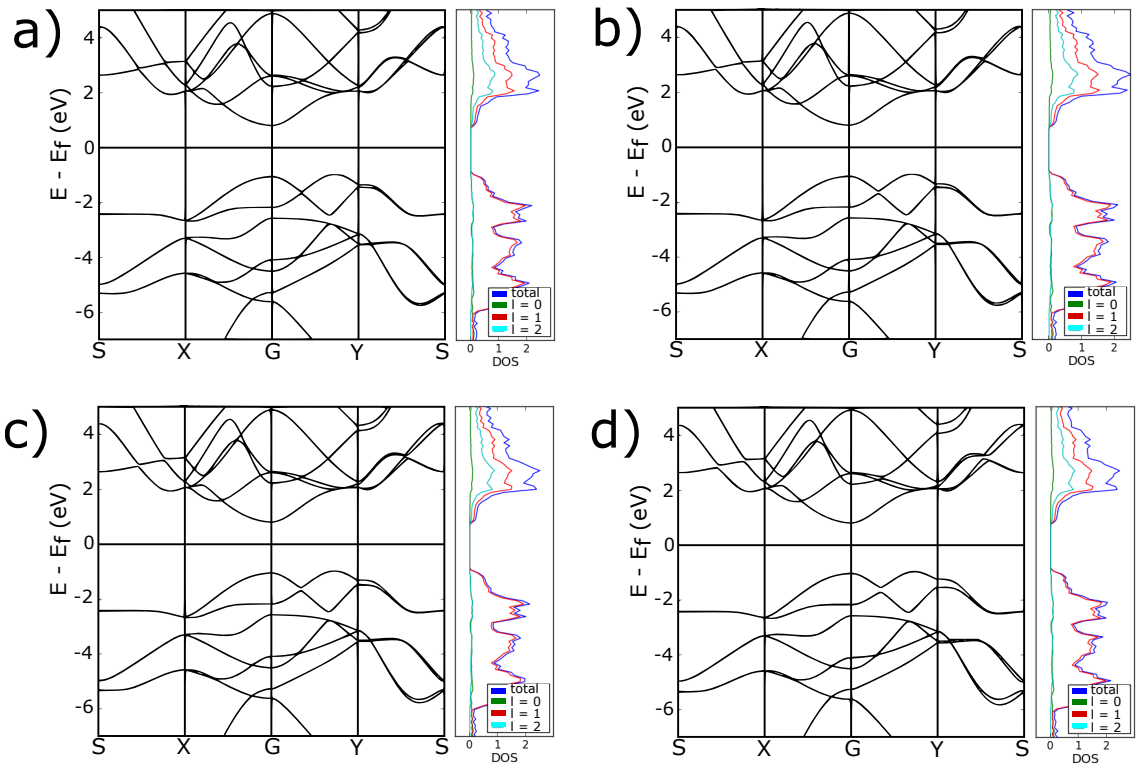

Figure 9. Bending in ac-direction causes band splitting in Y-S path. Splitting is more modest compared to zz-bending in figure 10. The radii of curvature in the images are: a) 121 Å, b) 94 Å, c) 67 Å and d) 40 Å.

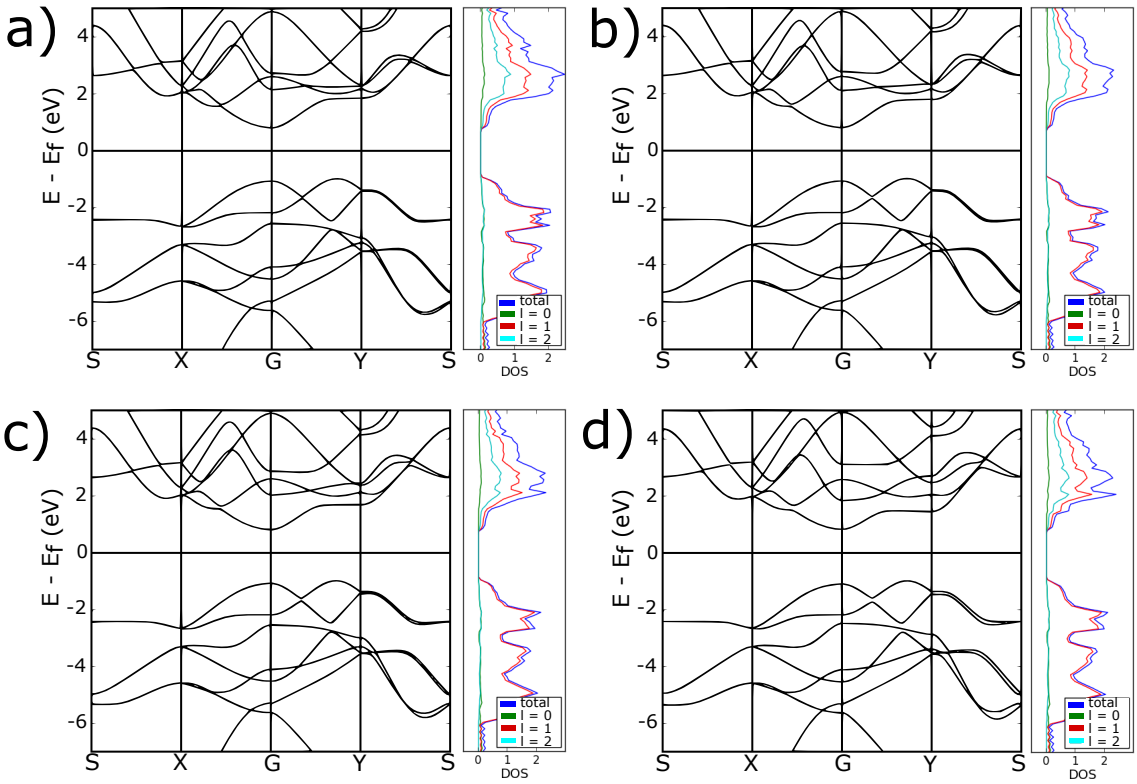

Figure 10. Bending in zz-direction causes clear changes in the Y-S path. There are similarities to shearing. Especially lines in negative energies are opening similarly in Y-S path as in shearing in figures 6 and 7. The radii of curvature in the images are: a) 97 Å, b) 75 Å, c) 54 Å and d) 32 Å.

Chiral bendings cause changes also in S-X path as seen in figure 11. When bending direction diverges from either ac- or zz-direction keeping curvature constant, splitting happens in S-X path. Along the S-X there are splitting parts that are also seen during shearing in figures 6 and 7. There is a notable relation between shear and bending. It has to be noted that all splitting phenomena are not identical to shearing. Pure shear does not cause splitting directly in X and Y points. The deformations caused by shear are also affected by the curvature, which naturally are seen as different alterations in band structure. There cannot be exactly similar effects in straight and curved sheets.

Verma *et al.* [14] presented the stress-strain relation in a matrix form as

$$\begin{pmatrix} \epsilon_c \\ \epsilon_t \\ \epsilon_{ct} \end{pmatrix} = \begin{bmatrix} \frac{1}{Y_c h} & \frac{-\nu_t}{Y_t h} & \frac{\eta_c}{Gh} \\ \frac{-\nu_c}{Y_c h} & \frac{1}{Y_t h} & \frac{\eta_t}{Gh} \\ \frac{\eta_c}{Gh} & \frac{\eta_t}{Gh} & \frac{1}{Gh} \end{bmatrix} \begin{pmatrix} \sigma_c h \\ \sigma_t h \\ \sigma_{ct} h \end{pmatrix}. \tag{66}$$

Here $Y_i h$ is Young's modulus, Gh shear modulus, ν_i Poisson ratio, $\sigma_i h$ plain stress and η_i is shear-strain coupling coefficient. Lower indices tell the direction. First c determines the direction of the quantity and t is perpendicular to it. Authors list that ϵ_c, ϵ_t and ϵ_{ct} describe layer extension along the direction c, layer compression in perpendicular direction and shear deformation respectively. According to them h is not required when in-plane elasticity is studied but it is necessary for out-of-plane bending. They point out that in 0° and 90° angles, which means in their case zz- and ac-directions, the shear-strain coupling coefficients vanish. This seems to be reflected in the band structure in S-X path. Bending in zz- and ac-directions does not cause any changes but splitting becomes visible immediately after diverging from these direction. These band structures agree with the result of Verma *et al.*.

The amount of applied bending in this study is relatively small compared to the studies of phosphorene nanotubes [45–47]. Curvature is not enough to change the band gap from direct to indirect as seen in these other studies. On the other hand the size of the band gap is affected by the radius of curvature. Bending in ac-direction makes band gap to shrink but zz-bending increases it. Same kind of a behavior is observed also with chiral bending in figure 12.

Interestingly the direct band gap is proportional to $1/R_c^2$, where R_c is a radius of curvature. This was observed in every bending direction. Bending directly in zz-direction increased the band bap and bending in ac-direction decreased it. All the intermediate directions are between them. Close to the 40° chirality from the zz-direction the gap stays close to a constant. Small deviation from direct ac-bending doesn't have large effect but even slight deviations from zz-direction cause notable changes in the behavior of the gap. Data is presented in the figure 12. The slopes of the line fits are in the table 5.

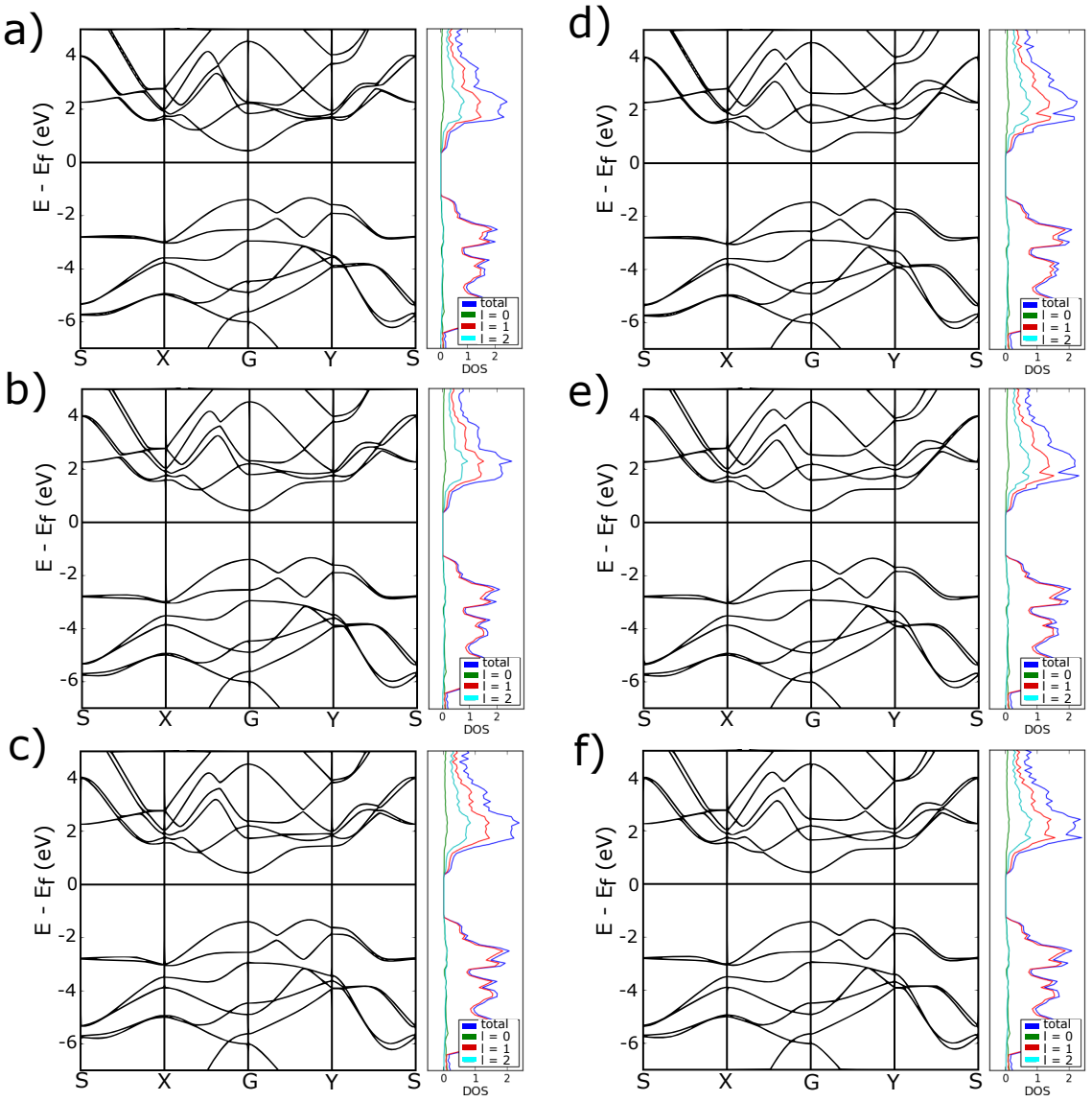

Figure 11. Bending in chiral directions causes band splitting along the S-X path. In every image the radius of curvature is 35 Å. The differences from the ac-direction are: a) 15°, b) 30° and c) 40°. The differences from the zz-direction are: d) 15°, e) 30° and f) 40°.

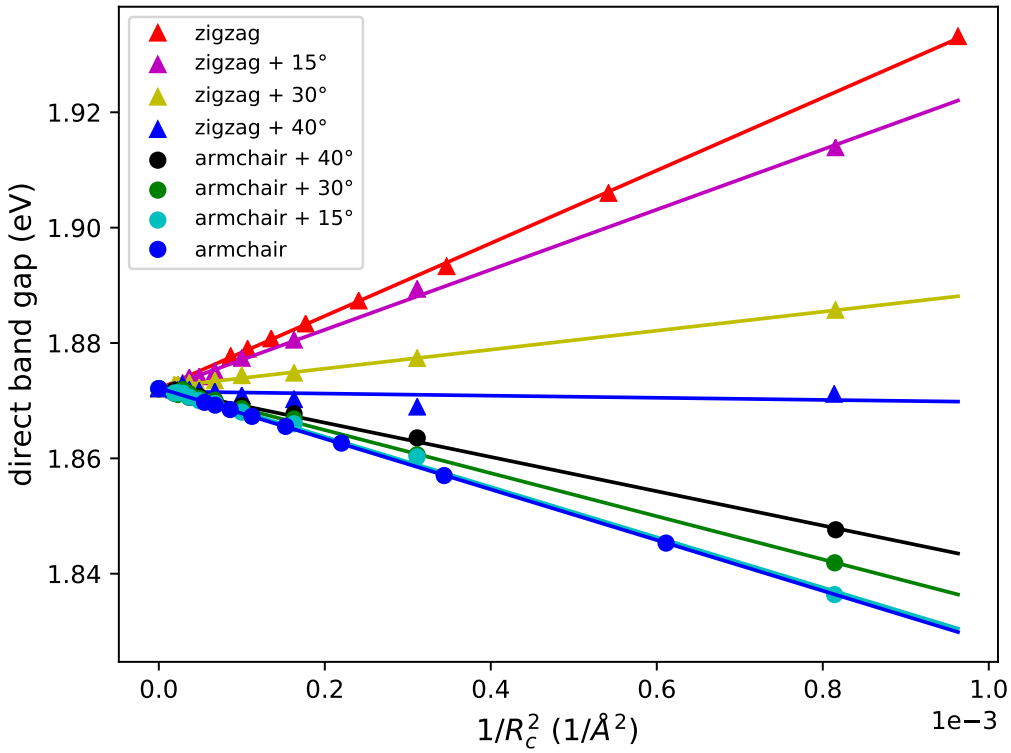

Figure 12. Direct band gap is linearly proportional to $1/R_c^2$. Fitted lines visualize this relation. Bending direction affects significantly to how direct band gap behaves during the bending.

Table 5. Direct band is linearly proportional to $1/R_c^2$ where R_c is the radius of curvature. Here are presented the slopes of the linear fits in figure 12. Interestingly the slope is closest to zero slightly before 40°, counting from zz-direction.

Direction	Slope (eV Å^2)
0° (zz)	63.098
15°	52.100
30°	16.451
40°	−1.826
50°	−29.722
60°	−37.372
75°	−43.592
90° (ac)	−43.945

Puckering makes phosphorene behave like it would have two layers. These layers behave differently if they are on outer or inner surface of the bent phosphorene sheet. On outer surface the layer stretches and on inner surface it is compressed. Between them there is a plane, which preserves its original measures during the bending. Ideally the plane is equally faraway from the both surfaces. The geometry of this situation is presented in figure 13.

The different behavior of outer and inner surface of the phosphorene sheet can explain the $1/R_c^2$ in some extent. The plane between the layers stays the same, so its length l is the original length of the both layers. Now the relative changes for the lengths of the outer and inner layers are

$$\frac{l_1 - l}{l} = \frac{\theta(R_c + d) - \theta R_c}{\theta R_c} = \frac{d}{R_c} \tag{67}$$

and

$$\frac{l_2 - l}{l} = \frac{\theta(R_c - d) - \theta R_c}{\theta R_c} = -\frac{d}{R_c}. \tag{68}$$

As we can see the relative changes are identical with opposite signs. Now the curvature is small and R_c is large. This leads the changes in l_1 and l_2 to be small. In the figure 5 it is seen that the direct band gap behaves linearly if the strain is small

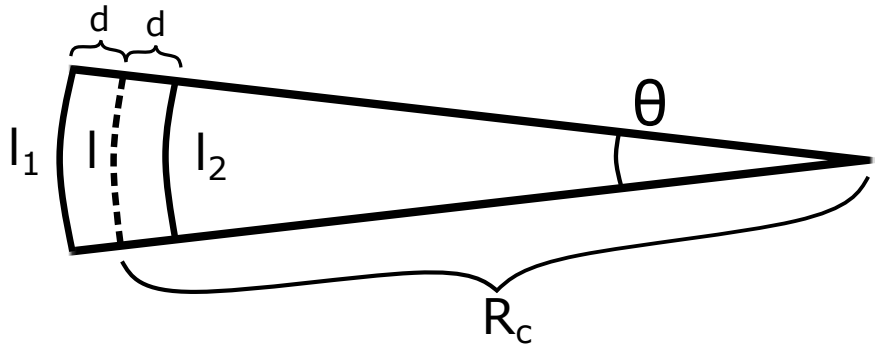

Figure 13. Here is the schematic picture about the bending of phosphorene sheet. Outer surface l_1 stretches and inner surface l_2 is compressed but l stays as a constant.

enough. Relative changes of the outer and inner surfaces are both proportional to $1/R_c$. This indicates that the strain is the same on both surfaces but with opposite signs. Because the linear dependence between the direct band gap and small strain, effects of inner and outer surfaces should cancel each other. In the end, if the direct band gap would be proportional to $1/R_c$, there would not be any changes in the direct band gap. In other words the band gap has to be proportional to higher order of the $1/R_c$. Now the square is the most significant term leading to $1/R_c^2$ dependence.

4.4 Mulliken population analysis

The phosphorene is considered as a two dimensional material. Still its puckered structure makes it behave like it would have two different layers, inner and outer one. Previously this explained the $1/R_c^2$ dependence of the direct band gap. The difference between outside and inside is also especially clear in mulliken populations when the structure is bent.

Shear does not cause significant changes in mulliken population even if it was 15% at maximum. Stretching causes some interesting changes. As seen in the figure 14a), stretching in ac-directions illustrates how the p and d orbitals are related to each other in both HOMO and LUMO states. While structure is compressed the p orbital contribution decreases in HOMO state and d orbital contribution increases. At the same time LUMO states behave the opposite way.

Phenomena in zz-stretching are not as smooth as in ac-stretching as seen in figure 14b). This is expected because phosphorene is more rigid in zz-direction than in

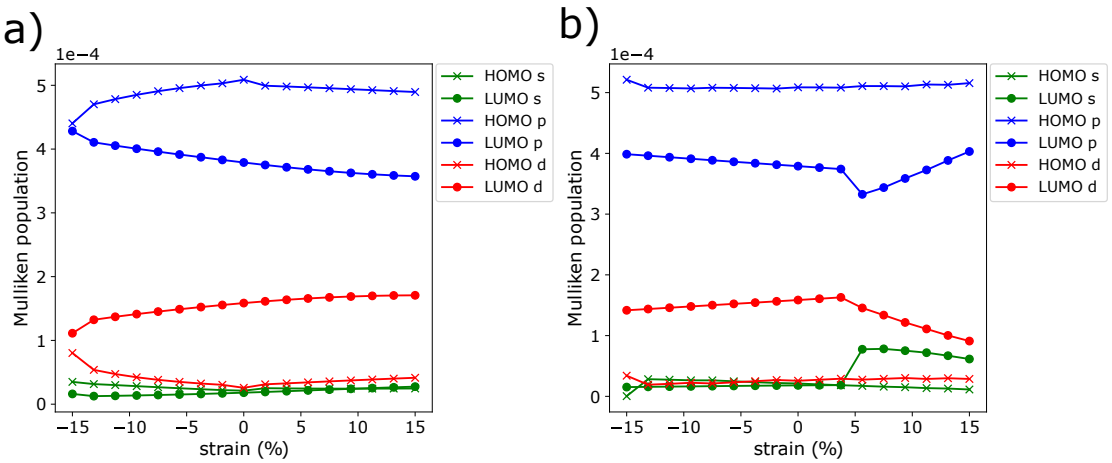

Figure 14. Stretching causes changes in the mulliken populations. In a) image stretching is done in ac-direction. In b) stretching is done in zz-direction. Changes are especially clear in zz-stretching.

ac-direction. Minor compression seems to cause similar behavior as described earlier in ac case. Actual stretching, on the other hand, transforms populations significantly already with about 7% strain. The changes happen mainly in LUMO side. There s orbital contribution increases sharply causing p orbitals to decrease. At the same time d orbital contribution begins to decrease linearly. After the most radical peaks s and d orbital contributions decrease and p increases. HOMO states experience only small changes.

Next figure 14b) is compared with the band structure in figure 4e) where stretching in zz-direction is about 5%. It is seen that there is a connection between mulliken population and band structure. When populations change sharply in the LUMO side, the band gap changes to indirect one. The lowest energy peak in the unoccupied side shifts from Γ towards Y. Now this can be explained with different orbital contributions. At the same time its worth checking the density of states (DOS) in figure 4e). Increasing the stretching increases the total DOS in LUMO side by "shrinking its tail" within the band gap region. This agrees well with mulliken populations. The sudden increase in s orbital populations and modest increase in p-orbital populations, after its drop, seem to be greater in total than the decrease in the d orbital populations.

Mulliken populations show that there is a connection between p and d orbitals. The behavior is easier to understand when the mulliken populations are associated

with wavefunction images in figures 15 and 16. These images are done by using Visual Molecular Dynamics (VMD) [48]. The electron densities or wavefunctions have been studied and imaged in several papers [17, 38, 42, 45, 49, 50], which gives a good material for comparison.

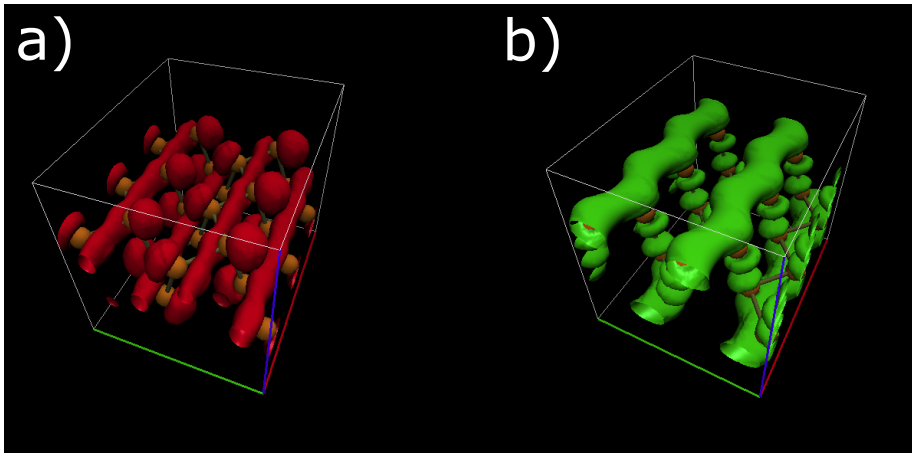

Figure 15. Here is the a) HOMO and b) LUMO orbitals of the phosphorene. Images are for the initial unstrained structure.

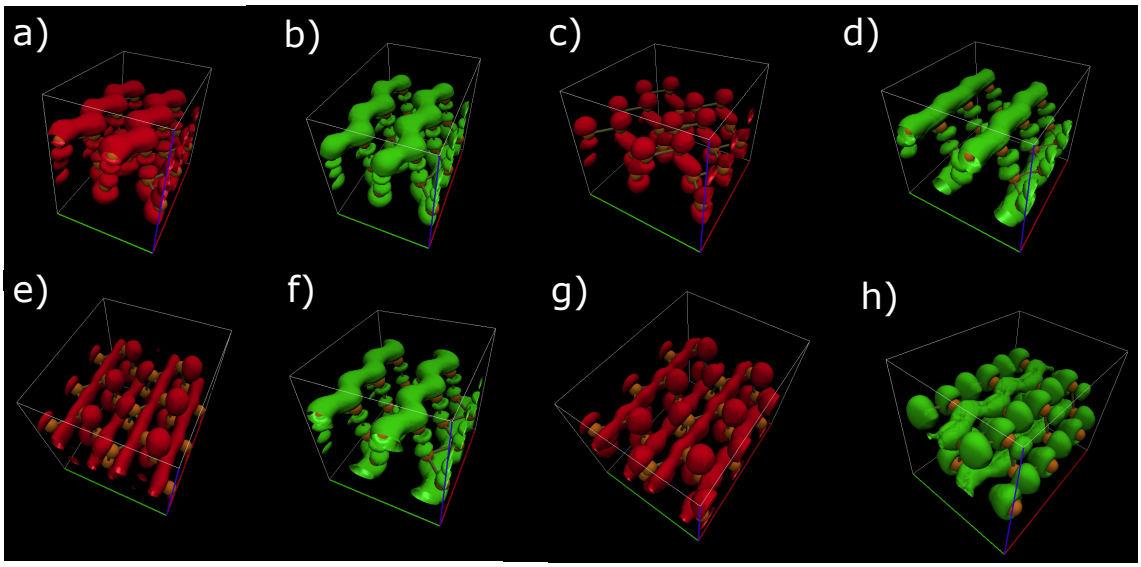

Figure 16. HOMO and LUMO states are shown for the stretched and compressed structures. In a) HOMO and b) LUMO phosphorene is compressed 15 % in ac-direction. In c) HOMO and d) LUMO phosphorene is stretched 15 % in ac-direction. In e) HOMO and f) LUMO phosphorene is compressed 10 % in zz-direction. In c) HOMO and d) LUMO phosphorene is stretched 10 % in zz-direction.

When stretching is 10% in zz-direction the LUMO states change. Without stretching the wavefunction was going along the bonded atoms in zz-direction but now it is between the puckers. Same time the mulliken population of the d-orbitals in LUMO has decreased greatly and p- and s-orbitals have more mulliken population. As mentioned earlier, this is the point when the lowest peak in unoccupied side shift from Γ towards Y. Even though the starting band gap was not direct due the parametrization it is clear that the gap becomes indirect. This kind of a transition has been reported by Peng, Wei and Copple [41].

Bending of phosphorene causes one major change in the mulliken populations as seen in figure 17. It is the difference between outer and inner surface of the layer. Changes in the p-orbitals of the HOMO state are the most apparent. When curvature increases the HOMO p orbital population moves from outer atoms to inner ones. The change in LUMO p orbitals' mulliken populations is opposite. The most likely reason for this is the change in the overlap of the orbitals. In inner surface the overlap is much stronger than in the outside. Bending in ac-direction bring the

puckers closer to each other in inner surface. This probably enables p orbitals to have better orientation and overlap making them more favorable on inner surface. This would increase their population in HOMO side. In zz-direction atoms are bonded more tightly and overlap is initially greater than in ac-direction. In this case it is logical that the corresponding changes in p orbital contributions are smaller than in the case of ac-bending as seen in figure 17b).

It has to be mentioned that bending in zz-direction affects not only to p orbitals but also to d orbitals. This is different compared to bending in ac-direction where mainly HOMO p orbitals are affected. In ac-direction orbitals have space to move, but in zz-direction overlap between orbitals is a significant factor. In zz-direction the alteration is seen in HOMO p, LUMO p and LUMO d. In LUMO states the outer p and inner d orbitals have more contribution than their counterparts. HOMO p orbitals were discussed earlier.

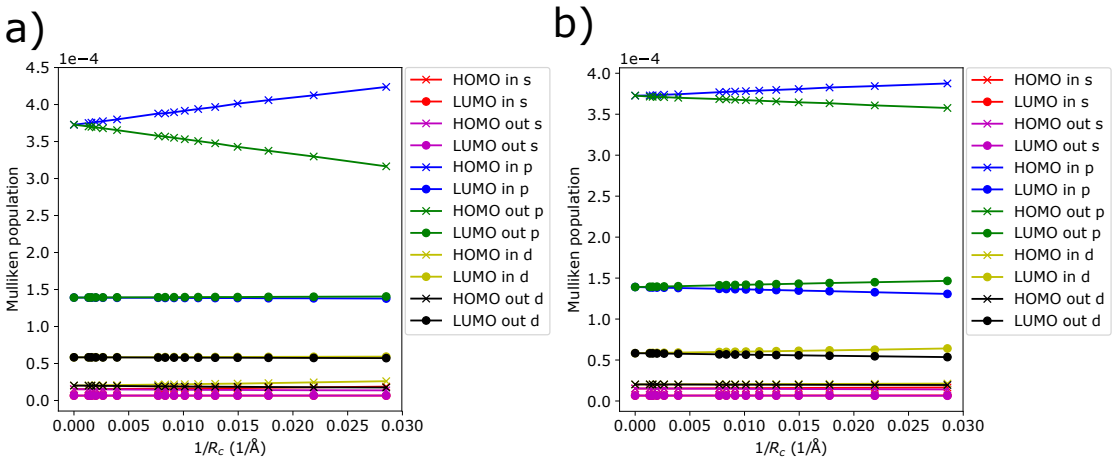

Figure 17. Mulliken populations for bending are presented as a function of $1/R_c$, where R_c is the radius of curvature. In a) bending is done in ac-direction and in b) it is in zz-direction. Coloring indicates which side of the phosphorene sheet is in question. Crosses indicate HOMO states and circles are for LUMO states.

5 Conclusions

Phosphorene or single-layer black phosphorus is a promising 2D material. Unlike graphene it has a tunable band gap making it a semiconductor. There have been numerous studies about its mechanical and electronic properties. Most of the research has been computational, but experimental results are also revealing how phosphorene could be exploited. One possible application seems to be FETs [7, 8] because of the useful semiconducting properties. On the other instance it has been shown that it is crucial to protect phosphorene from the oxygen and moisture. Despite its stability phosphorene forms easily oxides changing the properties significantly [11, 12].

Although there are some difficulties concerning parametrization, DFTB is a valid method to simulate phosphorene in elastic deformations. Absolute values might vary but qualitative analysis in trends is working. This is already mentioned by Koskinen and Mäkinen [18] when representing DFTB and Hotbit. In the section 3 many computed properties were compared to literature values. This shows that elastic properties agree especially well with earlier research even if there are some differences in bond lengths, bond angles and lattice constants.

The behaviour of the band structure during bending showed remarkable relations to shear. Along the S-X and Y-S paths the splitting of the bands was observed during the bending. This is the main change in band structure caused by shear. This study showed that the splitting in S-X is observed only with chiral bending directions. Results agree with the matrix presentation of Verma *et al.* [14] which is shown in equation (66). They stated that stress-strain coefficients vanish in ac- and zz-directions but otherwise affect to the system. This is exactly what is observed in S-X path while phosphorene is bent.

Sa *et al.* have reported that shear can change the band bap from direct to indirect [17]. This is due to band splitting. They point out that one possible application for this property is the shear strain protecting nanoelectronic switches. Bending causes similar band splitting, but the phenomenon is not as strong as in a case of pure shear. If phosphorene is subjected to bending in this kind of applications it is crucial to know whether the direct-to-indirect transition could happen. Allec and Wong

report that in certain sized phosphorene nanotubes band gap changes from direct to inderect [45]. This emphasizes that the knowledge about the the relation between bending and shear also concern the study of phosphorene nanotubes. Their design is not as simple as it looks like, because shear affects also to nanotubes' mechanical and electronic properties.

References

[1] C. E. Housecroft and A. G. Sharpe. *Inorganic Chemistry*. 4th ed. Pearson Education, 2012. ISBN: 978-0-273-74275-3.

[2] P. W. Bridgman. "Two new modifications of phosphorus". In: *Journal of American Chemical Society* 36 (7 1914), pp. 1344–1363. DOI: 10.1021/ja02184a002.

[3] K. S. Novoselov et al. "Electric Field Effect in Automatically Thin Carbon Films". In: *Science* 306 (5696 2004), pp. 666–669. DOI: 10.1121/science.1102896.

[4] C. Berger et al. "Ultrathin Epitaxial Graphite: 2D Electron Gas Properties and a Route toward Graphene-based Nanoelectronics". In: *Journal of Physical Chemistry B* 108 (52 2004), pp. 19912–19916. DOI: 10.1021/jp040650f.

[5] V. Tran et al. "Layer-controlled band gap and anisotropic excitons in few-layer black phosphorus". In: *Physical Review B* 89.23 (2014). DOI: 10.1103/PhysRevB.89.235319.

[6] H. Liu et al. "Phosphorene : An Unexplored 2D Semiconductor with a High Hole Mobility". In: *ACS Nano* 8.4 (2014), pp. 4033–4041. DOI: 10.1021/nn501226z. URL: http://pubs.acs.org/doi/abs/10.1021/nn501226z.

[7] L. Li et al. "Black Phosphorus Field-effect transistors". In: *Nature Nanotechnology* 9 (2014), pp. 372–377. DOI: 10.1038/nnano.2014.35.

[8] M. Buscema et al. "Fast and Broadband Photoresponse of Few-Layer Black Phosphorus Field-Effect Transistors". In: *Nano Letters* 14 (6 2014), pp. 3347–3352. DOI: 10.1021/nl5008085.

[9] F. Xia, H. Wang, and Y. Jia. "Rediscovering black phosphorus as an anisotropic layered material for optoelectronics and electronics". In: *Nature Communications* 5 (2014). DOI: 10.1038/ncomms5458.

[10] A. Castellanos-Gomez. "Black Phosphorus: Narrow Gap, Wide Applications". In: *The Journal of Physical Chemistry Letters* 6 (21 2015), pp. 4280–4291. DOI: 10.1021/acs.jpclett.5b01686.

[11] S.-L. Yau et al. “STM (010) surface of orthorhombic phosphorus”. In: *Chemical Physics Letters* 198.3 (1992), pp. 383–388. DOI: http://dx.doi.org/10.1016/0009-2614(92)85069-M.

[12] A. Ziletti et al. “Oxygen Defects in Phosphorene”. In: *Physical Review Letters* 114 (4 2015). DOI: 10.1103/PhysRevLett.114.046801.

[13] J. D. Wood et al. “Effective Passivation of Exofoliated Black Phosphorus Transistors against Ambient Degradation”. In: *Nano Letters* 14 (12 2014), pp. 6964–6970. DOI: 10.1021/nl5032293.

[14] D. Verma et al. “Directional-dependent thickness and bending rigidity of phosphorene”. In: *Physical Review B* 94 (12 2016). DOI: https://doi.org/10.1103/PhysRevB.94.121404.

[15] O. O. Kit, L. Pastewka, and P. Koskinen. “Revised periodic boundary conditions: Fundamentals, electrostatics, and the tight-binding approximation”. In: *Physical Review B* 84.15 (2011). DOI: 10.1103/PhysRevB.84.155431.

[16] T. Dumitrică and R. D. James. “Objective molecular dynamics”. In: *Journal of the Mechanics and Physics of Solids* 55 (10 2007), pp. 2206–2236. DOI: 10.1016/j.jmps.2007.03.001.

[17] B. Sa et al. “The electronic origin of shear-induced direct to indirect gap transition and anisotropy diminution in phosphorene”. In: *Nanotechnology* 26.21 (2015). DOI: 10.1088/0957-4484/26/21/215205.

[18] P. Koskinen and V. Mäkinen. “Density-functional tight-binding for beginners”. In: *Computational Materials Science* 47.1 (2009), pp. 237–253. DOI: 10.1016/j.commatsci.2009.07.013. URL: http://dx.doi.org/10.1016/j.commatsci.2009.07.013.

[19] https://github.com/pekkosk/hotbit. accessed 5.2.2018.

[20] https://wiki.fysik.dtu.dk/ase/. accessed 5.2.2018.

[21] P. Hohenberg and W. Kohn. “Inhomogeneous electron gas”. In: *Physical Review* 136.3B (1964), pp. 864–871.

[22] J. C. Slater and G. F. Koster. “Simplified LCAO method for the periodic potential problem”. In: *Physical Review* 94.6 (1954), pp. 1498–1524. DOI: 10.1103/PhysRev.94.1498.

[23] R. M. Martin. *Electronic Structure Basic Theory and Practical Methods*. Cambridge University Press, 2004. ISBN: 978-0-521-53440-6.

[24] R. G. Parr and W. Yang. *Density-Functional Theory of Atoms and Molecules*. Oxford University Press, 1989. ISBN: 0-19-509276-7.

[25] N. Bernstein, M. J. Mehl, and D. A. Papaconstantopoulos. "Nonorthogonal tight-binding model for germanium". In: *Physical Review B* 66.7 (2002). DOI: 10.1103/PhysRevB.66.075212. URL: http://link.aps.org/doi/10.1103/PhysRevB.66.075212.

[26] D. Porezag, T. Frauenheim, and T. Köhler. "Construction of tight-binding-like potentials on the basis of density-functional theory: Applications to carbon". In: *Physical Review B* 51 (19 1995). DOI: 10.1103/PhysRevB.51.12947.

[27] J. Junquera et al. "Numerical atomic orbitals for linear-scaling calculations". In: *Physical Review B* 64 (23 2001). DOI: 10.1103/PhysRevB.64.235111.

[28] R. S. Mulliken. "Electronic Population Analysis on LCAO-MO Molecular Wave Functions. I". In: *The Journal of Chemical Physics* 23.10 (1955). DOI: 10.1063/1.1740588.

[29] I. Mayer. *Simple Theorems, Proofs, and Derivations in Quantum Chemistry*. Kluwer Academic/Plenum Publishers, 2003. ISBN: 0-306-47409-3.

[30] C. Kittel. *Introduction to Solid State Physics*. 6th ed. John Wiley & Sons, 1986. ISBN: 0-471-87474-4.

[31] P. Koskinen and O. O. Kit. "Efficient approach for simulating distorted materials". In: *Physical Review Letters* 105.10 (2010). DOI: 10.1103/PhysRevLett.105.106401.

[32] M. E. Rose. *Elementary theory of angular momentum*. 1st ed. John Wiley & Sons, 1967.

[33] M. Gaus et al. "Parameterization of DFTB3/3OB for sulfur and phosphorus for chemical and biological applications". In: *Journal of Chemical Theory and Computation* 10.4 (2014), pp. 1518–1537. DOI: 10.1021/ct401002w.

[34] G. Qin et al. "Hinge-like structure induced unusual properties of black phosphorus and new strategies to improve the thermoelectric performance". In: *Scientific Reports* 4 (2014). DOI: 10.1038/srep06946.

[35] Q. Wei and X. Peng. “Superior mechanical flexibility of phosphorene and few-layer black phosphorus”. In: *Applied Physics Letters* 104.25 (2014). DOI: 10.1063/1.4885215. URL: http://dx.doi.org/10.1063/1.4885215.

[36] X.-B. Li et al. “Structure, stabilities and electronic properties of defects in monolayer black phosphorus”. In: *Scientific Reports* 5 (2015). DOI: 10.1038/srep10848.

[37] Y. Takao and A. Morita. “Electronic Structure of Black Phosphorus: Tight Binding Aproach”. In: *Physica B+C* 105 (1--3 1981), pp. 93–98. DOI: https://doi.org/10.1016/0378-4363(81)90222-9.

[38] J. Qiao et al. “High-mobility transport anisotropy and linear dichroism in few-layer black phosphorus”. In: *Nature Communications* 5 (2014). DOI: 10.1038/ncomms5475. URL: http://www.nature.com/ncomms/2014/140721/ncomms5475/full/ncomms5475.html?WT.ec%7B%5C_%7Did=NCOMMS-20140723%7B%%7D5Cnhttp://www.nature.com/doifinder/10.1038/ncomms5475.

[39] J.-w. Jiang. “Anisotropic Young’s Modulus for Single-Layer Black Phosphorus: The Third Principle Direction Besides Armchair and Zigzag”. In: *arXiv:1503.00200 [cond-mat]* (2015). URL: http://arxiv.org/abs/1503.00200.

[40] H.-Y. Zhang and J.-W. Jiang. “Elastic Bending Modulus for Single-Layer Black Phosphorus”. In: *Journal of Physics D: Applied Physics* 48.45 (2015). DOI: 10.1088/0022-3727/48/45/455305. URL: http://iopscience.iop.org/article/10.1088/0022-3727/48/45/455305/pdf.

[41] X. Peng, Q. Wei, and A. Copple. “Strain-engineered direct-indirect band gap transition and its mechanism in two-dimensional phosphorene”. In: *Physical Review B - Condensed Matter and Materials Physics* 90.8 (2014), pp. 1–10. DOI: 10.1103/PhysRevB.90.085402.

[42] Z. S. Popović, J. M. Kurdestany, and S. Satpathy. “Electronic structure and anisotropic Rashba spin-orbit coupling in monolayer black phosphorus”. In: *Physical Review B* 92 (3 2015). DOI: 10.1103/PhysRevB.92.035135.

[43] L. Liang et al. “Electronic Bandgap and Edge Reconstruction in Phosphorene Materials”. In: *Nano Letters* 14 (11 2014), pp. 6400–6406. DOI: 10.1021/nl502892t.

[44] W. Setyawan and S. Curtarolo. “High-throughput electronic band structure calculations: Challenges and tools”. In: *Computational Materials Science* 49.2 (2010), pp. 299–312. DOI: 10.1016/j.commatsci.2010.05.010. URL: http://dx.doi.org/10.1016/j.commatsci.2010.05.010.

[45] S. I. Allec and B. M. Wong. “Inconsistencies in the Electronic Properties of Phosphorene Nanotubes: New Insights from Large-Scale DFT Calculations”. In: *Journal of Physical Chemistry Letters* 7 (21 2016), pp. 4340–4345. DOI: 10.1021/acs.jpclett.6b02271.

[46] L. Guan, G. Chen, and J. Tao. “Prediction of the electronic structure of single-walled black phosphorus nanotubes”. In: *Phys. Chem. Chem. Phys.* 18 (2016), pp. 15177–15181. DOI: 10.1039/C6CP01803C.

[47] H. N. Fernández-Escamilla, J. J. Quijano-Briones, and A. Tlahuice-Flores. “Chiral phosphorus nanotubes: structure, bonding, and electronic properties”. In: *Phys. Chem. Chem. Phys.* 18.18 (2016), pp. 12414–12418. DOI: 10.1039/c6cp01869f.

[48] W. Humphrey, A. Dalke, and K. Schulten. “VMD: Visual molecular dynamics”. In: *Journal of Molecular Graphics* 14.1 (1996), pp. 33–38. DOI: 10.1016/0263-7855(96)00018-5. URL: http://www.sciencedirect.com/science/article/pii/0263785596000185.

[49] R. Fei and L. Yang. “Strain-engineering the anisotropic electrical conductance of few-layer black phosphorus”. In: *Nano Letters* 14.5 (2014), pp. 2884–2889. DOI: 10.1021/nl500935z.

[50] X. Han et al. “Strain and Orientation Modulated Bandgaps and Effective Masses of Phosphorene Nanoribbons”. In: *Nano Letters* 14 (8 2014), pp. 4607–4614. DOI: 10.1021/nl501658d.